A Review on Micro-mechanical Testing of NiTi-Based Shape Memory Alloys

S. Sujith Kumar[1], Adya Charan Arohi[2] and Indrani Sen[2]* (ID)

Abstract | NiTi-based shape memory alloys are considered as potential candidates for various structural, functional and biomedical applications. This is particularly related to their unique characteristics such as pseudoelastic and shape memory effects. Considering the increasing demand of NiTi alloys in miniaturized devices, the small-scale deformation micro-mechanisms of such a material system is being thoroughly reviewed in this article. At the first hand, the fundamental characteristics of NiTi system is discussed briefly. The influence of different factors such as chemical composition, crystallographic phases and precipitates on the phase transformation and mechanical behavior of the material are emphasized next. Subsequently, an extensive overview is provided regarding the assessment of small-scale deformation behavior of NiTi alloys using two prime techniques: micro-pillar compression and instrumented nanoindentation. Pros and cons for both the characterization techniques are analyzed as well. Interestingly, uniaxial compression of the micro-pillar reveals the pseudoelastic behavior in the alloy with remarkable enhancement in martensitic transformation stress and plateau strain with respect to those observed from macro-scale testing. It is also evident from the studies that mechanical behavior of the material strongly depends on different crystallographic orientation. Contrary to the uniaxial compression, nanoindentation generates triaxial state of stress beneath the tip of indenter, which is likely to influence the deformation micro-mechanism for the NiTi system, as well. Variation in hardness, elastic modulus and recoverability of NiTi system are primarily assessed through nanoindentation-based studies. In addition, recent studies highlight the importance of optimizing the nanoindentation parameters such as tip configuration, tip radius and load level for precise estimation of pseudoelastic activity in the alloy. Moreover, a simplified approach is generated for estimating the indentation stress–indentation strain curve. Overall, this paper generates a thorough and comprehensive insight about the micro-mechanical testing of NiTi-based shape memory alloys.

1 Introduction

The last few decades have witnessed a widespread usage of miniaturized devices in various engineering applications. With significant modification in the lifestyle and societal need, there develops a growing demand for reducing the size scale of the common and essential devices, appliances, machineries, etc. for different kind of structural, functional

[1] Department of Metallurgical Engineering and Materials Science, Indian Institute of Technology, Bombay 400076, India.
[2] Department of Metallurgical and Materials Engineering, Indian Institute of Technology, Kharagpur 721302, India.
*indrani.sen@metal.iitkgp.ac.in

Springer

and biomedical applications. It is noteworthy that most of the miniaturized devices rely on employing materials with special properties resulting in outstanding performances. For instance, significant elastic recovery is crucial for the functioning of the cardiovascular stent inside the arteries[1]. Similarly, an alloy system that shows distinct and reversible variation of shape with temperature can be ideally used as micro-sensors in certain applications[1]. In fact, many such requirements utilize the exceptional characteristics of smart materials such as shape memory alloys (SMA). NiTi-based system, popularly known as NiTiNOL is the most widely used SMA, which exhibits exceptional elastic recovery, reasonably high strength as well as high damping capacity along with fairly good biocompatibility and corrosion resistance[2]. These superior structural and functional properties of NiTi-based SMAs have made them potential candidates for various niche components like Micro-Electro-Mechanical Systems (MEMS), microactuator, guide wires, orthodontic braces, orthopaedic staples, etc.[3–6]. However, for successful utilization and for the smooth functioning of these miniaturized components, it is important to ensure this exceptional combination of properties at such small scale.

In general, the localized mechanical performance of most of the materials is extrapolated from the corresponding global characteristics. Interestingly, the measured properties at the micro- and nano-scales differ distinctly from their macroscale counterparts[7–9]. As a consequence, it is always challenging to design a component in a sub-micron scale based on the understanding of the deformation behavior of the material from the bulk scale. This essentially highlights the necessity for developing thorough insight and employ specific characterization tools which are explicitly suitable to assess the small-scale deformation behavior of the material. Taking account of the relevance of the NiTi system for practical applications as well as for generating a scientific perspective, the present article aims to review the major studies on the deformation behavior of the NiTi system. The micro-mechanisms of deformation for the NiTi system at the small scale is particularly taken into consideration. To develop a comprehensive understanding, the metallurgical concepts related to NiTi-based SMA are discussed at the first hand.

2 Metallurgical and Mechanical Characteristics of NiTi-Based SMA

From the generic point of view, it is well known that variation in the state of stress/temperature causes the system to undergo different deformation modes to achieve minimum energy criterion. Traditional alloy systems attain the equilibrium criteria via two physical phenomena: (i) atomic bond stretching and relaxation, leading to elastic deformation, and (ii) bond rearrangement resulting in dislocation-mediated plasticity. The degree of these two atomic rearrangements primarily defines the overall mechanical response of the conventional alloy system, at a specific temperature[9–12]. Interestingly, apart from these conventional mechanisms, SMAs largely rely on thermoelastic martensitic phase transformation. Consequent to this, the mechanical properties of SMAs exhibit unique trends in stress–strain behavior compared to traditional metallic systems. In addition, the thermal characteristics of SMAs do reveal the signature of reversible phase transformation as well.

Various alloy categories, including NiTi, Ni–Ti–Cu, Fe–Mn–Si–Co–Ni, Fe–Mn–Si, Cu–Zn–Al, Cu–Al–Ni, Cu–Sn, etc. were reported to show the shape memory properties[9,13]. Among all these SMA systems, NiTi-based alloys are noted to exhibit superior structural and functional properties. The exceptional characteristics of NiTi system is primarily related to the martensitic transformation between the high symmetric parent austenite phase (B2 cubic structure) and the low symmetric product martensitic phase (B19' martensitic structure). It is noteworthy that the entire transformation between these two phases is governed by the activities of the corresponding variant pair (CVP)[14]. In fact, CVP refers to the number of possible ways in which the B2 austenite phase transforms to B19' martensite. Generally, any of 24 different CVP can activate in the NiTi system. Owing to this variation in the degree of symmetry to a large extent, the NiTi alloy depicts superior shape memory properties than other SMAs and hence most widely used for practical applications.

2.1 Shape Memory Properties of NiTi System

Based on the triggering source for the activation of martensitic transformation, shape memory properties are classified into two categories: (i) pseudoelastic effect (PE) and (ii) shape memory effect (SME). While PE can be achieved in SMA with the variation in applied stress at a particular temperature, SME depends on the variation of both the stress and temperature. In general, NiTi system at low temperature (in martensitic phase) depicts SME and at intermediate temperature (austenitic state) shows PE. On the other hand,
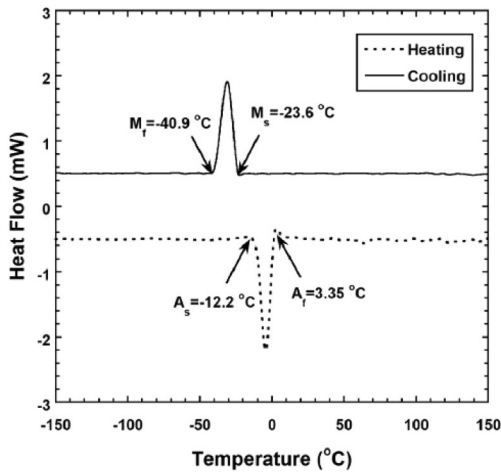
212

🍃 Springer

J. Indian Inst. Sci.|VOL 102:1|211–235 January 2022|journal.iisc.ernet.in

Figure 1: Differential scanning calorimetry thermogram showing phase transformation characteristics of the Ni-rich NiTi system (reproduced with permission from [16]).

the material behaves like a conventional elastic–plastic system at high temperature. To understand the potential of shape memory characteristics of SMA at a specific temperature, the transformation temperatures are analyzed using a differential scanning calorimetry (DSC) experiment. Figure 1 shows the temperature-induced phase transformation characteristics obtained from the

DSC thermogram of the NiTi system. This first-order transition defines the functional properties of the shape memory system[15]. The characteristic temperatures for the forward transformation from the austenite phase to the martensite phase commences and finishes at M_s and M_f respectively, upon cooling the NiTi system. On the other hand, heating the alloy leads to a reverse transformation to the parent austenite phase that starts and ends at A_s and A_f, respectively. Distinct peaks representing the unique phase transformation characteristics with all these temperatures are indicated in Fig. 1. More details about the shape memory properties are elaborated below:

2.1.1 Pseudoelasticity (PE)

Ideally, SMA consisting of austenite phase at the experimental temperature (ET) is expected to depict PE. The typical stress (σ)–strain (ε) characteristics of the pseudoelastic NiTi alloy during tensile deformation are presented in Fig. 2a. With the application of stress, elastic deformation of the parent austenitic phase (B2 phase) prevails following Hooke's relationship (see segment AB in Fig. 2a). Next, at a critical stress level, stress-induced martensitic transformation (SIMT) commences. Micromechanisms controlling the SIMT in SMAs are completely governed by the twinning process, rather than the slip activities
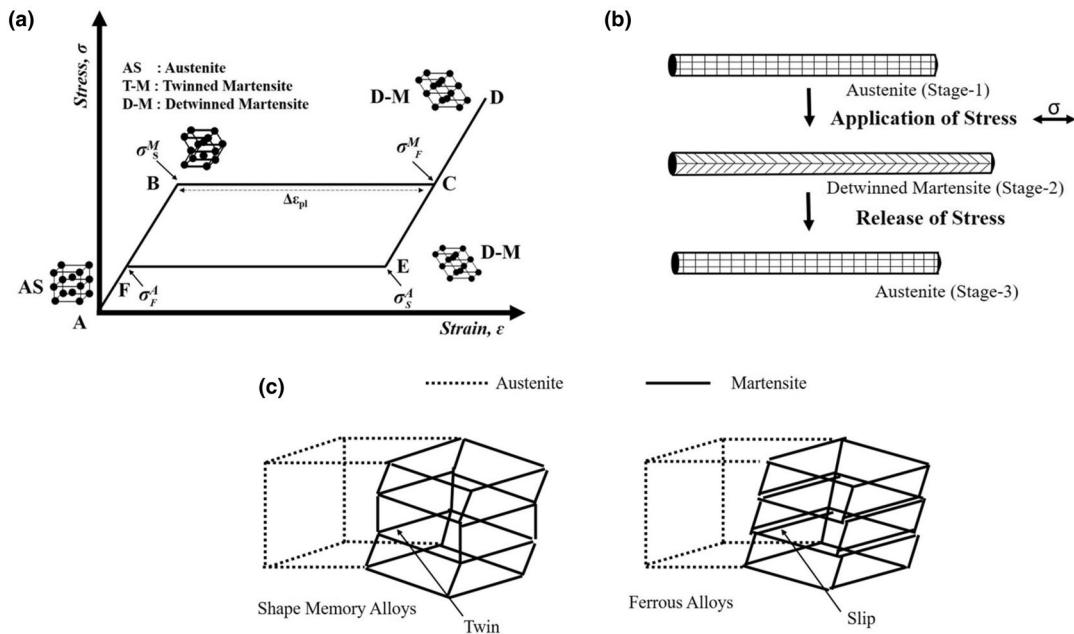

Figure 2: **a** Stress–strain–temperature diagram showing pseudoelastic effect in NiTi-based alloys. **b** Macroscopic changes during the pseudoelastic effect[22], **c** schematic representation of the atomic rearrangement for martensitic transformation in shape memory alloys and ferrous alloys.

213

J. Indian Inst. Sci.|VOL 102:1|211–235 January 2022|journal.iisc.ernet.in

as noted in the traditional metallic systems, say ferrous alloy[15]. Owing to this unique reversible transformation mode, SMA could regain its original shape in macro-scale, unlike the permanent deformation observed in ferrous alloys during the SIMT. Figure 2c shows the difference in martensitic transformation between the shape memory alloys and ferrous alloys. The stress required to initiate such transformation process is termed as martensitic start stress, σ^M_S, indicated by point B. At this point, the austenite phase starts transforming into the twinned martensite phase (B19' phase). σ^M_S of NiTi system, as estimated from bulk-scale uniaxial testing, is reported to be in the range of (300–500) MPa[17–19]. The transformed martensite phase next de-twins. In the detwinning process, the self-accommodating variants of martensites transform into the one oriented along the direction of applied stress[20]. Also, this detwinning process is observed to be much easier than the activation of austenite slip[21]. This leads to considerable increment in the strain with nominal influence in the corresponding stress level. This mechanism is reciprocated in securing a strain plateau segment, $\Delta\varepsilon_{pl}$ in the σ–ε curve, shown by a dashed double-sided arrow in Fig. 2a. This detwinning process completes at a stress level of σ^M_F (martensitic finish stress, indicated by C in Fig. 2a).

Overall, the atomic-level changes in the lattice in terms of transformation and detwinning contribute towards a macroscopic shape alteration in the material. This is reflected as segments A–B–C in Fig. 2a and schematically illustrated in Fig. 2b as stage I and II. Subsequent loading deforms the detwinned martensite elastically, and it follows the segment CD in the σ–ε curve. The unloading from point D will lead to elastic recovery of the martensite phase at the first instance. Furthermore, reverse transformation to austenite phase initiates at σ^A_S (austenite start stress), indicated by an arrow at E and completes at σ^A_F (austenite finish stress) indicated by F in Fig. 2a. Upon further unloading, elastic recovery of the austenite phase materializes and the specimen gets back to the position A in Fig. 2a. The overall recoverable deformation activity generates the hysteresis loop in the stress–strain curve, as a signature trend for pseudoelastic material. The complete shape recovery is apparent from stage-III in Fig. 2b. Owing to the recoverable and reversible SIMT in association with the conventional elastic mechanism, the NiTi system shows strain recovery (8–10%) that is almost an order of magnitude higher than that realized for any elastic–plastic alloy systems (maximum 1%)[2]. This extensive strain recoverability in NiTi alloy; which is typically related to elastic deformation in standard elastic–plastic materials; is coined as 'pseudoelasticity' (or superelasticity) in SMAs. From the application point of view, the PE for the NiTi system is exploited for the design of cardiovascular stents, superelastic tires for lunar rover, optometric glass frames, orthodontic braces, etc.[23,24].

2.1.2 Shape Memory Effect (SME)

SME is essentially realized through sequential thermal and stress-induced phase transformations. Figure 3a illustrates the shape memory effect of NiTi alloy through the stress–strain–temperature (σ–ε–T) diagram[25]. The three steps associated with the process are:

i. Forward transformation of austenite into twinned martensite by cooling, represented by segment AB in Fig. 3a. Owing to the self-accommodated variant formations in the twinned martensite, this stress-free process is devoid of macroscopic deformation into the material (see 'Stage-I and Stage-II' in Fig. 3b).

ii. Next, elastic deformation of the twinned martensite (indicated by segment BC) results through the application of stress. Subsequently, upon achieving the critical stress, σ^M_S, detwinning (reorientation) of the twinned martensite commences through the activation of particular martensitic CVP. The detwinning process completes at σ^M_F, and leads to a strain plateau, $\Delta\varepsilon_{pl}$ represented by segment CD in Fig. 3a. Further application of stress results to recoverable elastic deformation of the detwinned martensite phase, indicated by segment DE in Fig. 3a. The overall alteration in shape is represented by 'Stage-III' in Fig. 3b.

iii. Upon unloading, the deformation of the martensite phase recovers as evident from segment EF in Fig. 3a. Finally, upon heating the detwinned martensite phase to a temperature above A_F, the backward thermoelastic transformation to the austenite phase results, as per the segment FA in Fig. 3 (a). Consequently, the initial shape of the specimen is regained, as shown by 'Stage-IV' in Fig. 3b[26]. This overall phenomenon in SMA is known as one way shape memory effect (OW-SME).

214

Springer

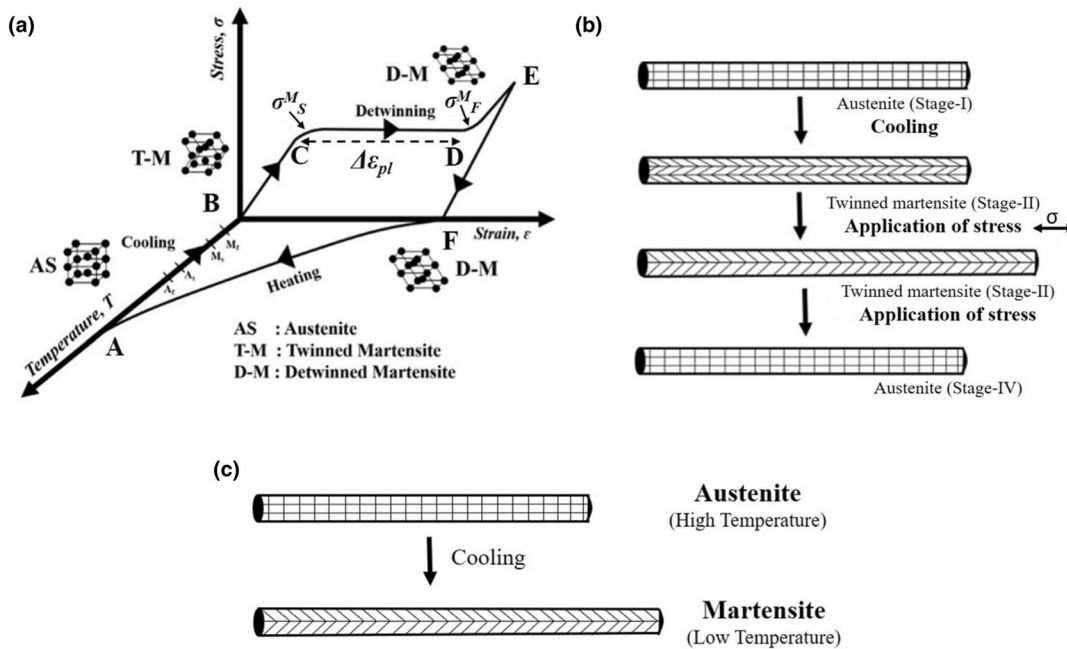J. Indian Inst. Sci.|VOL 102:1|211–235 January 2022|journal.iisc.ernet.in

Figure 3: a Stress–strain–temperature diagram showing shape memory effect in NiTi-based alloys. **b** Macroscopic changes in the material associated with reversible phase transformation[15], **c** schematic representation of macroscopic changes associated with two-way shape memory effect.

Apart from OW-SME, SMAs can exhibit two-way shape memory effect (TW-SME) also. TW-SME refers to the ability of the material to remember two different shapes both at austenite phase at higher temperature and at martensite phase at lower temperature. Figure 3c schematically demonstrates the shape changes associated with TW-SME in NiTi system. In fact, as per TW-SME, NiTi alloys can acquire shape change to the predefined ones even without application of stress. It is basically achieved by performing a certain cyclic thermomechanical treatment known as "training". Upon repetitive training for large number of cycles, the microstructure of NiTi alloys alters significantly. It generates specific microstructures associated with the stress field. This stress field directs variants of CVPs to activate in the temperature-induced martensitic transformation. It is believed that either residual martensite or dislocations generated from cyclic training is the main reason for TW-SME[27].

2.2 Factors Influencing the Deformation Behavior of the NiTi System

For the practical usage of the NiTi-based *SMAs*, it is important to comprehend the factors that critically control the micro-mechanisms of deformation. It is observed that any variation in the alloy composition, phase constituents, transformation temperatures, etc. strongly alters the mechanical performance of the material[28–30]. The role played by each of these factors affecting the deformation characteristics of the NiTi system are described briefly:

2.2.1 Composition

It is noteworthy that slight alteration in the composition with respect to the equiatomic NiTi alloy leads to substantial variations in both the PE and SME characteristics. Figure 4 shows the partial phase diagram of NiTi system. In NiTi system, the Ni-rich composition (50.1–52 at% Ni) is known to depict pseudoelastic properties at room temperature (RT). Excess nickel is noted to strongly depress the forward (martensitic) transformation temperatures leading to occurrence of austenite phase at RT[31]. For instance, in case of solutionized NiTi alloy, an increase in the Ni content by 1 at% (from 50.6 to 51.6 at%) results to a reduction in the M_S temperature from 280 K to below 100 K, thereby making the alloy favorable to exhibit PE at RT[32,33]. On the other hand, in case of the aged alloy, owing to the resistance offered by precipitate against the dislocation movement, occurrence of precipitates appears beneficial in improving the mechanical performance of the
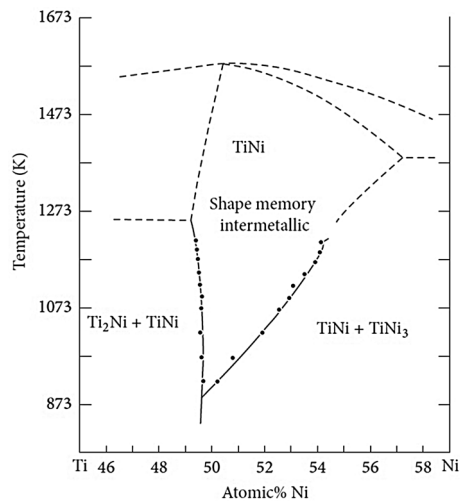
Figure 4: Partial equilibrium phase diagram of NiTi system (reproduced with permission from[35]).

Table 1: Characteristic properties of phases present in NiTi system[33,36].

Phase	Yield strength (MPa)	Elastic modulus (GPa)
Austenite	195–690	41–75
Martensite	70–250	28–41
R-phase	5–25	–

alloy. The Ti–rich NiTi system, however, shows increased transformation temperature as compared to that for the Ni-rich system, leading to the stability of martensite phase at RT. Therefore, Ti-rich systems are preferred for applications that utilize the SME of the NiTi system[34].

2.2.2 Crystallographic Phases

Unique functional characteristics of NiTi alloy are controlled by the existence of different crystallographic phases in the alloy as well as their transformation behavior. In fact, the different phases of the NiTi system yield distinctly varying mechanical properties. The range of yield strength and elastic modulus of the austenite, martensite and *R*-phases of NiTi alloys, as determined through uniaxial tensile tests are mentioned in Table 1. Primarily, three different phases in the NiTi system play key roles in controlling the functional characteristics and thereby mechanical behavior of the alloy. Amongst these, the role of cubic B2 austenite and monoclinic B19' martensite phases are already mentioned in the previous sections. In addition, the occasional occurrence of an intermediate metastable rhombohedral *R*-phase is also noted in the NiTi system.

Crystal structures of these mentioned phases in NiTi alloy are shown in Fig. 5a. The parent austenite phase, stable at a comparatively higher temperature has the ordered intermetallic structure of CsCl (space group: Pm3m)[37]. R-phase is the rhombohedral distortion and the martensite phase is the monoclinic (space group: P2₁/m) distortion of this parent austenite phase[38]. The

nature and characteristics of transformation between these phases play a significant role in defining the overall mechanical behavior of the NiTi system. Therefore, it is explained in detail below.

The forward transformation (B2–B19' or B2–R) is associated with the reduction in Young's modulus and leads to lattice softening of the system. Formation of either B19' or R-phase during forward transformation is solemnly governed by the thermodynamic and kinematic factors. Martensite is formed when the thermodynamic factors control the atomic rearrangement. However, in some cases, kinematic factors take over the thermodynamics and form the R-phase. The presence of the local stress field in the matrix accounts for this formation. Some instances for the generation of local stress field includes the presence of Ni-based precipitates (in aged Ni-rich NiTi system, as discussed in the next section); addition of alloying elements such as Fe, Al, Co; generation of dislocations after cold working, etc. All these can enable the formation of R-phase[39]. In these cases, further cooling/stress is necessary to convert the metastable R-phase into B19' phase. However, in most cases, the reverse transformation is associated with the direct transformation of martensite back to the austenite phase. This is termed as a single-stage backward transformation from B19'→ B2. Few exceptions have been reported where the reverse transformation is noted to occur via the R-phase. This, therefore, leads to multiple stage transformation (B19'→ R → B2). In general, quenched samples depict single-step transformation and aged samples show multiple-step transformations[36]. Overall, occurrence of all these phases and their relative contents at a temperature of interest play important roles in modifying the mechanical performance of the alloy system.

From a crystallographic point of view, martensitic transformation in NiTi system is governed by activation of CVP. In NiTi system, the
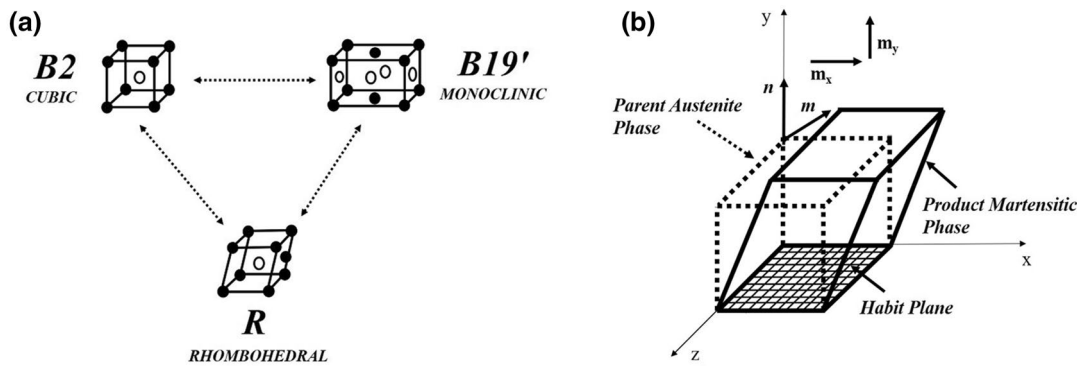
216

Springer

J. Indian Inst. Sci.|VOL 102:1|211–235 January 2022|journal.iisc.ernet.in

Figure 5: a Schematic representation of different phases of NiTi alloy. **b** Schematic representation of the martensitic transformation and associated crystal changes of a single crystal austenite of NiTi alloy[40].

Table 2: Precipitate phases of NiTi system with corresponding crystallographic shape and lattice parameters[34,41].

Precipitate	Shape	Lattice parameter
Ni_4Ti_3	Rhombohedral	$a = 0.67$ nm, $\alpha = 113.9°$
Ni_3Ti	Hexagonal close packed	$a = 2.5505°A$, $c = 8.3067A°$
$NiTi_2$	Face-centered cubic	$a = 11.278$ A°

transformation of the higher symmetric parent cubic phase to the lower symmetric product monoclinic phase can occur along any of 24 possible CVPs[40]. Figure 5b represents the CVP activation associated with the martensitic transformation from single-crystal austenite. Crystallographic parameters of B2 crystal structure with habit plane normal, $n = \{-0.8889, 0.2152, 0.4044\}$ and transformation direction, $m = \, <0.4144, 0.7633, 0.4981>$ represents one CVP[13]. On the other hand, the permutation and combination of these crystallographic parameters provide other 23 CVPs that can lead to a similar transformation of B2 to B19' phase. Figure 5b shows the crystal structure changes associated with the activation of one variant. In Fig. 5b, n denotes the unit vector normal to the habit plane, and m denotes the direction of transformation. The m_x and m_y denote the resolved components of transformation strain along the x and y directions, respectively. Shear strain component m_x leads to shear, whereas m_y denotes expansion of the crystal at a direction perpendicular to the habit plane[40]. The symmetric variations and associated transformation between the parent and product crystal structures of a particular *SMA* govern structural and functional characteristics of NiTi system.

2.2.3 Influence of Precipitates

Changes in the overall composition as well as the thermomechanical heat treatments adopted to the NiTi alloy system result to precipitate formations. Precipitates such as Ni_4Ti_3, Ni_3Ti, and $Ni_{14}Ti_{11}$ are normally noticed to evolve in the Ni-rich NiTi alloy system. On the contrary, $NiTi_2$ is noted to form in the Ti-rich alloy[41–43]. A heat treatment below 680 °C is generally adopted to evolve precipitates in the matrix[44]. In fact, detailed understanding about the role of aging parameters in evolving the different precipitates in NiTi system can be obtained from the systematic investigations pursued by Duerig et al.[36]. The crystal structure and the lattice parameters of the most commonly observed precipitate phases for NiTi system are tabulated in Table 2. The presence of these micro- to nano-sized precipitates generate strain incompatibilities with other constituent phases in the material. Consequently, internal stress develops in the matrix. The coherency of the precipitate–matrix interfaces along with the distribution of precipitates within the matrix primarily govern the amount of stress fields that generate. Among the different precipitate morphologies, coherent precipitates are expected to generate a higher stress field than the semi-coherent and incoherent ones[45]. This phenomenon can

Springer

be better appreciated from Fig. 6. The dotted lines (region *A*) in the vicinity of the precipitate in the schematic reveals the existence of localized stress fields, σ_{loc} while the matrix (region *B*) is devoid of such field. It is noteworthy that *SIMT* proceeds across the zone where the applied shear stress reaches a critical value (σ_S^M) required for the activation of a particular *CVP*. Hence, region *A* surrounding the precipitate is more susceptible to initiate martensitic transformation in the NiTi matrix, at the first hand. In other words, precipitates help to reduce the external shear stress needed for the transformation[14]. Further, stress field around the precipitate leads to formation of *R*-phase by rhombohedral distortion of the cubic phase austenitic phase[26].

This ease of phase transformation in presence of precipitates is also reflected in enhancing/diminishing the corresponding martensitic transformation temperature as well. Such influence on the martensite transformation is governed by the nature of stress state around the precipitate in the matrix. M_S of the NiTi system is expected to increase with the occurrence of Ni-rich precipitates in the matrix. Further, localized compositional variation also significantly influences the overall characteristics of the NiTi system. This can also lead to alteration in the M_S temperature of a particular alloy[2]. In fact, precipitates being a different phase in comparison to the NiTi matrix is not capable to undergo the unique reversible transformation features. Practically, an increase in the volume fraction of the precipitates reduces the capability of the alloy system to undergo reversible transformation. Essentially local stress field and compositional variations modify the functional properties of the NiTi system[14].

All these unique mechanical and thermal characteristics of the NiTi system are evident from its global behavior[21]. However, to deploy *SMA* in various applications on a sub-micron-scale, documenting the material behavior on such a small scale is highly imperative. In this regard, a significant number of studies have already addressed the influence of size effect on the overall performance of traditional alloys systems[46–51]. It is observed that, with the reduction in the size scale, the elastic–plastic system shows improved strength[52–54]. Nevertheless, apart from the conventional mechanisms, the reversible martensitic transformation plays a significant role in controlling the mechanical response of the NiTi system, as well. Various attempts in this regard are mentioned below.
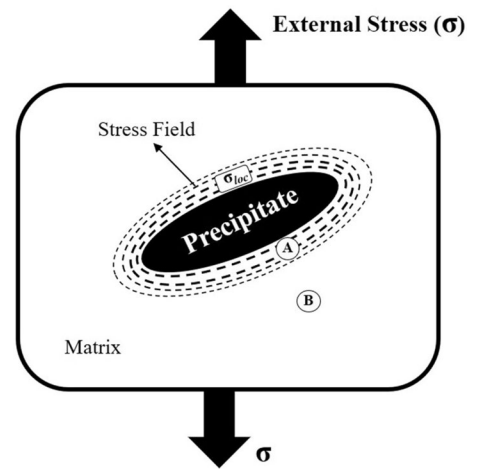

Figure 6: Schematic demonstration of the precipitate acting as the local (internal) stress field adding up with the applied (external) stress[14].

3 Assessment of Small-Scale Deformation Behavior of NiTi System

Considering the increasing usage of NiTi-based SMAs for miniaturized devices and appliances, this particular section focuses on reviewing the state-of-the-art research on the (sub) micro-scale shape memory characteristics and mechanical performance of the material. It is, however, noteworthy that precise characterization of the properties at such small scale are limited to a fewer techniques, owing to the complications in the experimentation methodologies[48]. Amongst these, (i) Micro-pillar compression and (ii) Nanoindentation are the most widely adopted characterization methods for the same. While the former applies an uniaxial mode and maintains a constant area throughout the experiments, the latter accounts for triaxial state of stress beneath the indenter tip with a varying contact area. These two techniques in general are designed to extract the nature of elastic and plastic activities in any materials. However, implementing these characterization tools for the NiTi system need special attention. This is particularly because the occurrence of SIMT in the alloy complicates the elementary deformation modes. Furthermore, it is important to develop a thorough understanding on the effect of decreasing size scale on the SIMT and PE behavior of NiTi-based SMAs. Several scientific investigations have been pursued on the NiTi system in the last two decades. Selected studies that have impacted the field largely and succeeded in generating important insights are discussed here.

218

Springer

J. Indian Inst. Sci.|VOL 102:1|211–235 January 2022|journal.iisc.ernet.in

3.1 Micro-pillar Compression Test of NiTi-Based SMAs

Recent advancements in the fabrication process with precise control on critical dimensions have made experimental execution at sub-micron length scales practically feasible. Uchic et al. were the first to demonstrate a novel technique for estimating the small-volume mechanical behavior of materials by virtue of uniaxial compression of micro-pillars[50]. Focused ion beam (FIB) is the prime technique to fabricate micro-pillars of required dimensions from the bulk materials. This technique uses a high-energy ion beams (Ga^+, Xe^+, He^+) which are bombarded on the sample of interest to sputter on the uppermost layer of a material. This experimental method is based on milling of micron-sized pillars of diameters varying in the range of 140 nm–5 μm with an aspect ratio (height to diameter) of 2–3[49–51,55–58]. In general, Ga^+ ion is used to machine the micro-pillar with diameter of nanometer ranges. Subsequently, compression of the pillars in a nanoindenter with a flat diamond punch is executed and the corresponding deformation responses are recorded. Accordingly, the mechanical properties of the material of interest are estimated. This whole method of the experiment is in similitude with the traditional uniaxial test in terms of the absence of strain gradient during the deformation.

Various scientific groups have reported on micro-pillar compression tests, often combined with subsequent theoretical analysis, to evaluate the martensitic transformation behavior of SMAs[47,55,59–61]. These previous investigations mostly considered the pseudoelastic strain range and the corresponding size and orientation effects therein. In pseudoelastic NiTi systems, a study based on the size scale was initiated by Frick et al.[55]. Compression tests on aged NiTi alloy were executed by them typically on micro-pillars of diameters varying over a wide range, from a few tens of microns down to less than 200 nm. This study had shown the influence of Ga^+ ion in modifying the micro-pillar surface and thereby influencing the property assessment. Most importantly, the investigation by Frick et al. is pioneer in revealing many unique features in stress–strain curves as an indication of functional activity in the NiTi system at the sub-micron scale[55]. For example, significant strain recovery along with hysteresis in the stress–strain curve confirmed the pseudoelastic activity in the material, even at such a small scale. Nevertheless, the stress–strain characteristics of the NiTi system in (sub) micron scale

was observed to be drastically different from the corresponding macro-scale behavior. In case of the former, the martensitic transformation was observed to initiate at significantly higher stress (> 1000 MPa) as compared to the reported value for the macro-scale (300–500 MPa)[17–19]. In addition, substantial plasticity generated in micro-pillar with a diameter less than 200 nm, upon deforming up to the same extent. On the basis of this systematic study, it was concluded that diameter of 200 nm as the critical limit for the activity of SIMT mechanism in the NiTi system. Figure 7 highlights the stress–strain behavior of NiTi alloy, using micro-pillar compression test depicted by Frick et al.[55].

Contradictory to this study, occurrence of SIMT during compression of pillars with diameters even < 200 nm was confirmed with the aid of in situ transmission electron microscopy (TEM) and diffraction pattern analyses[59]. Figure 8a, b highlight the TEM image of micro-pillar compression and associated phase changes during the deformation of NiTi system. Accordingly, Ye et al. investigated the small-scale deformation behavior of the NiTi system through micro-pillar compression test[59]. They varied the diameter of the pillars in the range of 140–200 nm. The precipitate-free NiTi system in the fully austenitic phase was used for this particular study. Such an alloy is most adequate to reveal pseudoelasticity. Additionally, Ye et al. implemented in situ TEM along with micro-pillar compression to record the microstructural changes associated with the phase transformation and its reversibility in a more reliable manner[59]. This complimentary technique provided reliable evidence for the evolution of SIMT in the NiTi system even for a size scale below 200 nm and revoked the observation, reported by Frick et al.[55]. It is noteworthy that the misinterpretation of deformation behavior of NiTi alloy by Frick et al. was mainly due to the inability in differentiating the signature of SIMT and the noise present in data while using the ex situ micro-pillar test[55]. On the other hand, Ye et al. had overcome it by continuously evaluating the diffraction patterns during the compression of micro-pillar in in situ TEM mode[59]. Further, multi-step transformation was observed during the loading of the micro-pillar. Nevertheless, it is noted that, while ex situ tests can be misleading, in situ tests, by virtue of direct observation, are advantageous in characterizing the stress-induced deformation mechanisms in SMA. In situ micro-pillar bending studies have also been performed by different groups on NiTi alloy both with and without precipitates. The primary aim was to
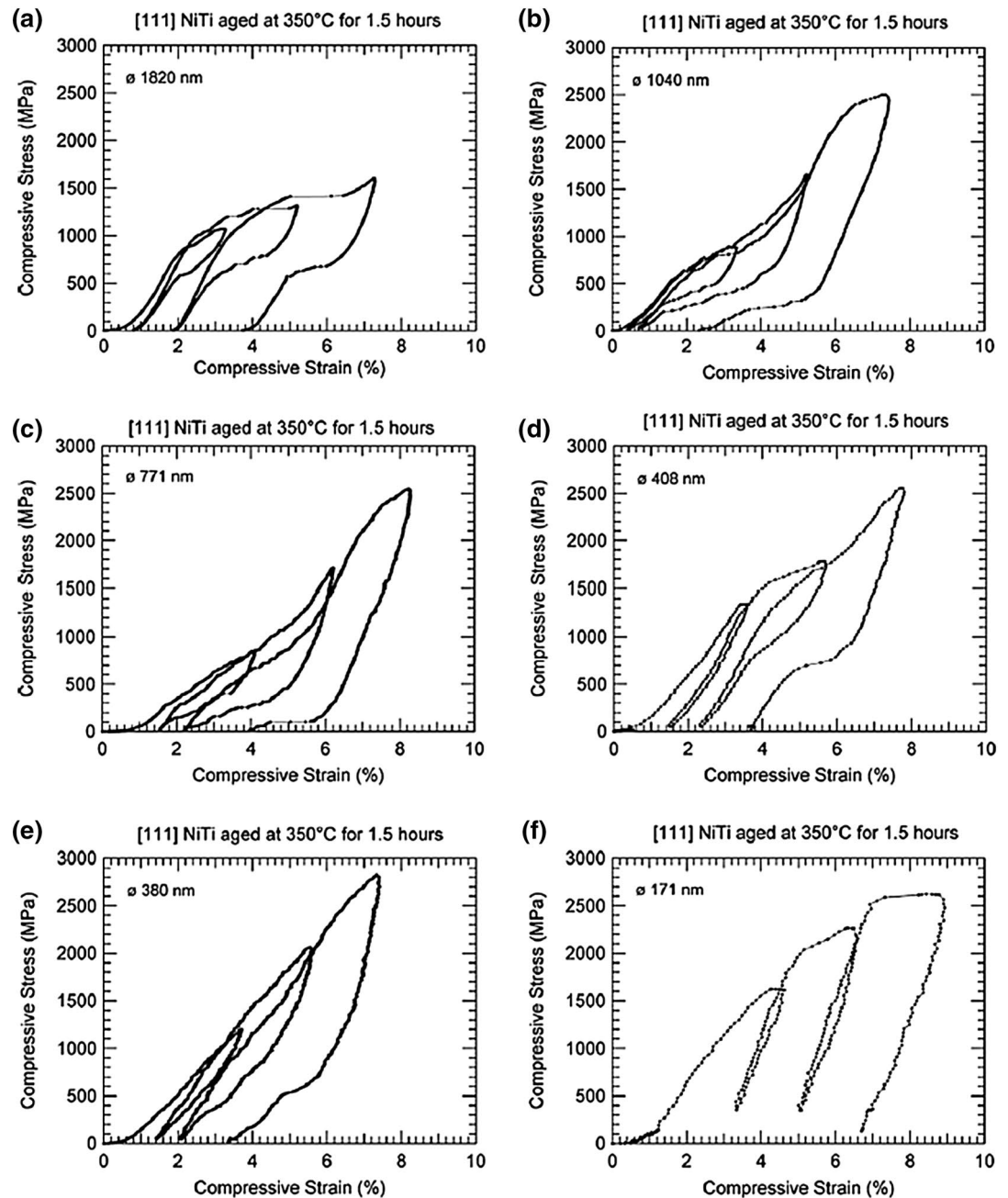
Figure 7: Stress–strain behavior of NiTi system obtained upon compressing micro-pillars of varying diameters and aging conditions (reproduced with permission from[55]).

study the effect of different initial microstructures on small-scale pseudoelasticity of the alloy[47,62,63].

Overall, SIMT was noted to instigate at a much higher stress during micro-pillar compression in comparison to that observed from bulk-scale testing. The fully recoverable strain limit was estimated to be as high as 15% at the nano-scale[55]. It is noteworthy that almost double the strain recovery with a reduction in size scale is strongly influenced by the deformation of the substrate below rather than from micro-pillar

itself. Hence, the experimental artifacts in modifying the true characteristics of the material should be well considered as well.

In addition to this experimental evaluation, Paul et al. investigated the crystallography–microstructure correlation of NiTi system in small scale[64]. This simulation-based study analyzed the influence of grain size as well as crystallographic orientations on the deformation response of NiTi micro-pillar. A steep strain gradient is observed in case of the large grain sized (421 nm) micro-pillar
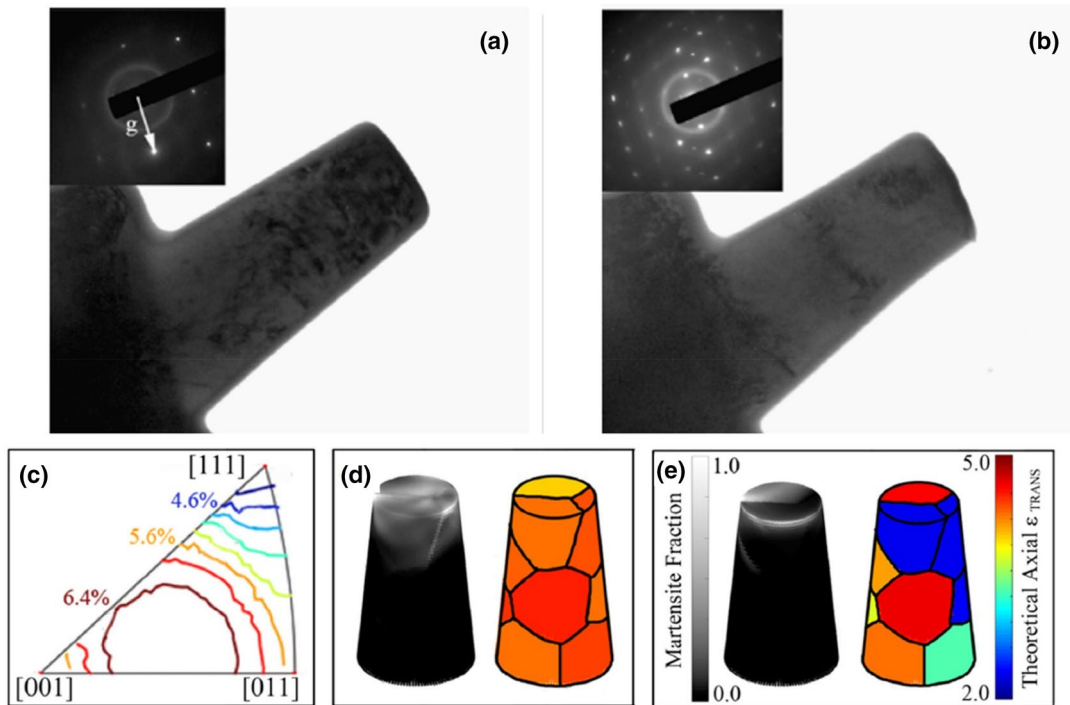
220

Springer IISc

J. Indian Inst. Sci.|VOL 102:1|211–235 January 2022|journal.iisc.ernet.in

Figure 8: TEM bright field image of FIB milled NiTi micro-pillar **a** before and **b** after compression up to engineering strain of 20%. Insets in the figures reveal the diffraction spots corresponding to **a** B2 austenite phase and **b** B19' martensitic phase (reproduced with permission from[59]), **c** stereographic triangle representing the transformation stain produced in differently oriented grains with respect to loading axis, (d) micro-pillar with cold-rolled, and **e** random texture. In both the specimen, the white region shows the deformation (reproduced with permission from[54]).

as compared to that noted for smaller grain sized (86 nm) pillar. It was demonstrated that such variation in the degree of strain within the micropillar is related to the variation in the deformation levels adjacent to the grain boundary as well as at the interior. Since grain boundaries act as potential sites for the initiation and propagation of deformation mechanism, the overall extent of deformation is noted to be significantly influenced by the grain size of the NiTi system. Moreover, variation in transformation strain (ε_{trans}) along the different crystallographic orientations of the micro-pillar is studied next. Figure 8c highlights the color-coded stereographic triangle representing ε_{trans} for each grain. This study clearly points out that randomly textured micro-pillar deforms to a higher extent in comparison to that noted for a cold-rolled texture. This is apparent from Fig. 8d, e.

In another attempt, the influence of crystallographic orientation on the stress–strain characteristics of the NiTi system was systematically examined by Pfetzing et al.[58]. This study primarily focused on compressing the principal orientations of NiTi system. The idea

was to assess the role of orientation of the austenitic phase on the deformation response of the alloy. Micro-pillars machined from the $< 111 >$, $< 101 >$ and $< 001 >$ orientations of Ni-rich NiTi alloy, were compressed to reveal unique observations as highlighted in Fig. 9. A significant anisotropy in stress–strain behavior resulted with variation in the crystallographic orientation. It is noted from this study that hysteresis in stress–strain curve, onset of martensitic transformation as well as estimated elastic moduli, etc. alter with variation in the crystallographic orientations. For instance, micro-pillars with $< 001 >$ and $< 101 >$ orientations deform with a distinct indication for SIMT in the corresponding stress–strain curves. In contrary, occurrence of SIMT is not so drastic and apparent for $< 111 >$ orientation. Also, complete strain recovery is never attained in micro-pillar orientated along $< 111 >$ direction. These observations suggested that while $< 001 >$ and $< 101 >$ crystallographic orientations are suitable for the occurrence of SIMT, $< 111 >$ orientation is mostly in favor to activate dislocation-mediated plasticity during
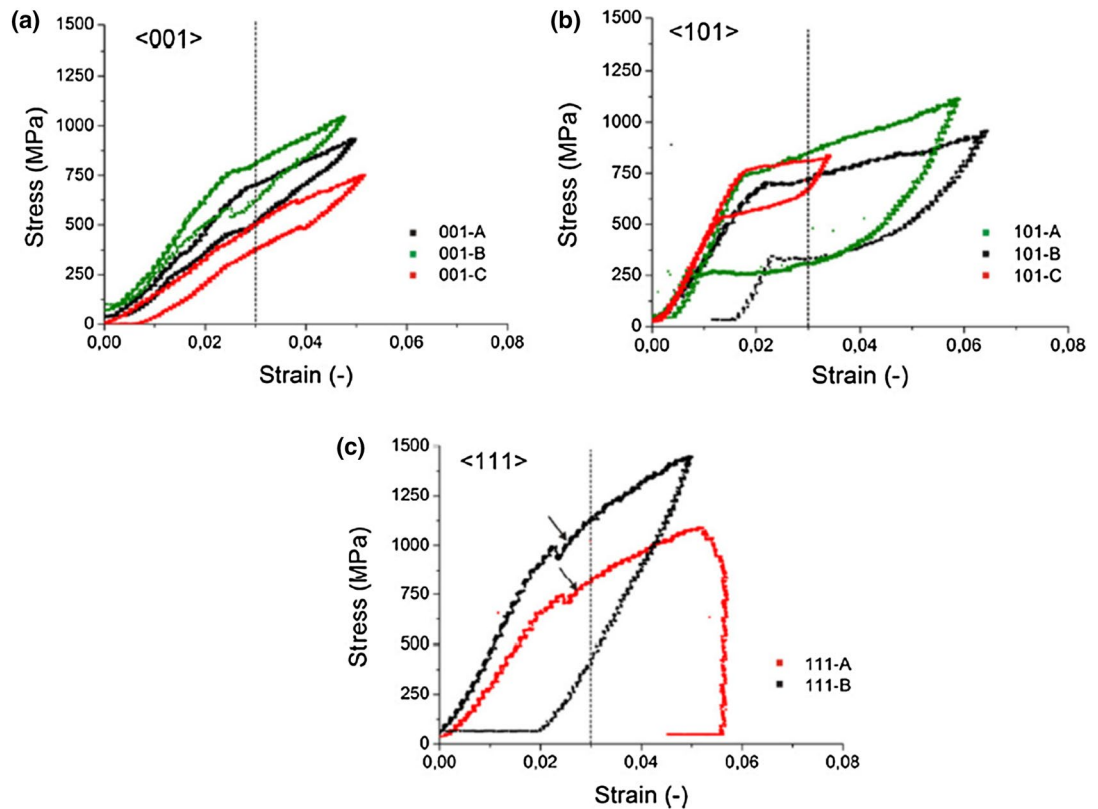
Springer

Figure 9: Stress–strain behavior of NiTi system obtained upon compressing micro-pillars, fabricated on principle orientations (reproduced with permission from[58]).

the deformation. In this regard, the investigation pursued by Pfetzing et al. highlighted the influence of crystallographic orientation on the deformation behavior of NiTi system in submicron scale[58]. This orientation related disparity in the stress–strain behavior of NiTi system is expected to be controlled by the inherent phase transformation mechanism. In fact, variation in strains for CVP formation and CVP detwinning between different crystallographic orientation is primarily reported from traditional uniaxial test for NiTi system[65].

Apart from these major studies, several other research groups have also investigated the small-scale deformation response of pseudoelastic NiTi system through micro-pillar compression[66–68]. Most of the studies in general agree with the aforementioned observations.

3.1.1 Challenges Associated with Micro-pillar Compression Test

The role of niche testing facility such as micro-pillar compression in evaluating the small-scale deformation behavior of NiTi-based SMAs is illustrated in the previous section. However, it is equally important to comprehend the challenges associated with this process: in terms of sample preparation and testing. At the first hand, the necessity of high-end facilities such as FIB for sample preparation and difficulties to obtain a precise micro-pillar has restricted the usage of such testing techniques, in general. Pillar tapering, surface damage, implantation and gallium damage are the most commonly reported issues during the preparation of micro-pillar. In addition to this, buckling/bending of pillars and errors in the alignment of the flat indenter punch are reported to influence the final stress–strain curve generated from the micro-pillar test[48]. Few reported issues in micro-pillar test are briefed here.

3.1.1.1 Pillar Tapering In general, it is extremely challenging to machine a micro-pillar with a uniform diameter throughout the length. A tapering of the pillar configuration results upon fabrication. This leads to a gradual increment in the diameter of the pillar from the top to the base. Hence, a non-uniformity in the applied stress level

222

🍃 Springer

J. Indian Inst. Sci.|VOL 102:1|211–235 January 2022|journal.iisc.ernet.in

prevails at the different sections of the pillar, which violates the uniaxial condition[48]. In practice, stress is usually estimated considering the diameter of the top section of the micro-pillar, resulting to an overestimation for the characteristic strengths[48]. In fact, considering the size scale of the pillar, even slight tapering of the sample results in a significant misinterpretation of the material behavior. This certainly influences estimating the true pseudoelastic characteristics of the material[55].

3.1.1.2 Formation of Ga⁺-Implanted Surface

Ga^+ ion is used for machining the micropillar from the material of interest. However, in the process, Ga^+ ion is prone to get implanted on the micro-pillar surface. This may in turn, modify the surface characteristics of the sample[48]. It is noteworthy that even with the application of a minimal beam current (~ 50 pA), absorption of Ga^+ on the sample surface is observed. A fractography study by Frick et al. reported occurrence of a thin layer (~ 17 nm) of Ga^+ on the surface of the NiTi micro-pillar[55]. This additional layer imparts some amount of strain upon deforming the pillar. Consequently, the precise pseudoelastic characteristics of the NiTi system is hampered.

3.1.1.3 Misalignment of Micro-pillar and Flat Punch

To obtain a gradual activation of different deformation modes in the material, strain gradient should be avoided. This can be realized through the uniaxial deformation of pillars by maintaining the proper alignment between the pillar surface and flat punch. Any error in alignment during the experimentation can alter the uniaxial stress state into multi-axial, thereby leading to misinterpretation of the mechanical properties[59].

3.2 Nanoindentation (NI)

Considering the experimental simplicity, NI technique has been widely utilized for characterizing the localized deformation behavior of the material. The high-resolution depth-sensor attached to the nanoindenter controls the deformation zone in sub-micron scale. Correspondingly, continuous variation in the indentation load (P) vs indentation depth (h) responses of the material are recorded when the specimen surface is penetrated by the rigid indenter. These responses are utilized to estimate the mechanical properties of the studied material. In general, mechanical properties like hardness (H) and elastic moduli

(E) are calculated using NI[69]. However, studies in later stages explored the potential of NI in evaluating the residual stress, dislocation density, phase transformation characteristics, shear band formation etc. from the P–h curve[70–72]. Several studies are also performed in a different line to evaluate the functional behavior of NiTi-based shape memory alloys using NI[73–76]. A few such pioneering studies are highlighted here:

3.2.1 Characterization of SME Behavior Using NI

NI has been employed as an important tool to characterize SME for NiTi thin films. Shaw et al. investigated the properties of NiTi thin films by nanoindenting at different load levels ranging from 0.5 to 8 mN[74]. The indent impressions were captured using atomic force microscope (AFM), shown in Fig. 10a. Subsequently, the specimens were heated to 200 °C, i.e., above its A_f temperature (70 °C) for 30 s. Consequently, the indentation stress-induced martensite phase reverted back to the austenite phase. Eventually, the indent impressions also disappeared, as evident from the corresponding image, presented in Fig. 10b.

Furthermore, stress-assisted deformation and temperature-induced shape recovery characteristics for martensitic NiTi thin films, subjected to not only nanoindentation but also nano-wear and nano-scratch tests were reported by Crone et al.[77]. Figure 10c, d shows the AFM topographical maps of nano-scratch before and after heating, respectively. It is apparent from the figure that scratch marks recovered to a large extent post-heating. In another study, Li et al. tried to estimate the A_f temperature of NiTiHf alloy by performing *NI* tests over a temperature range varying between 30 and 340 °C[78]. It was noted that hardness increased significantly from 2.8 GPa at 205 °C to 3.47 GPa at 230 °C. This signified that the low-temperature martensite phase transformed to austenite phase. They also proposed a technique to detect the transformation temperature using spherical indentation techniques. According to this technique, the particular temperature over a range that corresponds to the highest indentation depth during heating and cooling are considered as A_f and M_s, respectively. On the other hand, all the transformation temperatures were further determined by calculating the corresponding work recoverability ratio during heating and cooling, as well[78].

Apart from these studies, Zhang et al. investigated the TW-SME in NiTi alloy by implementing indentation with the ball and clamp method[79]. They clamped a tungsten carbide ball

223

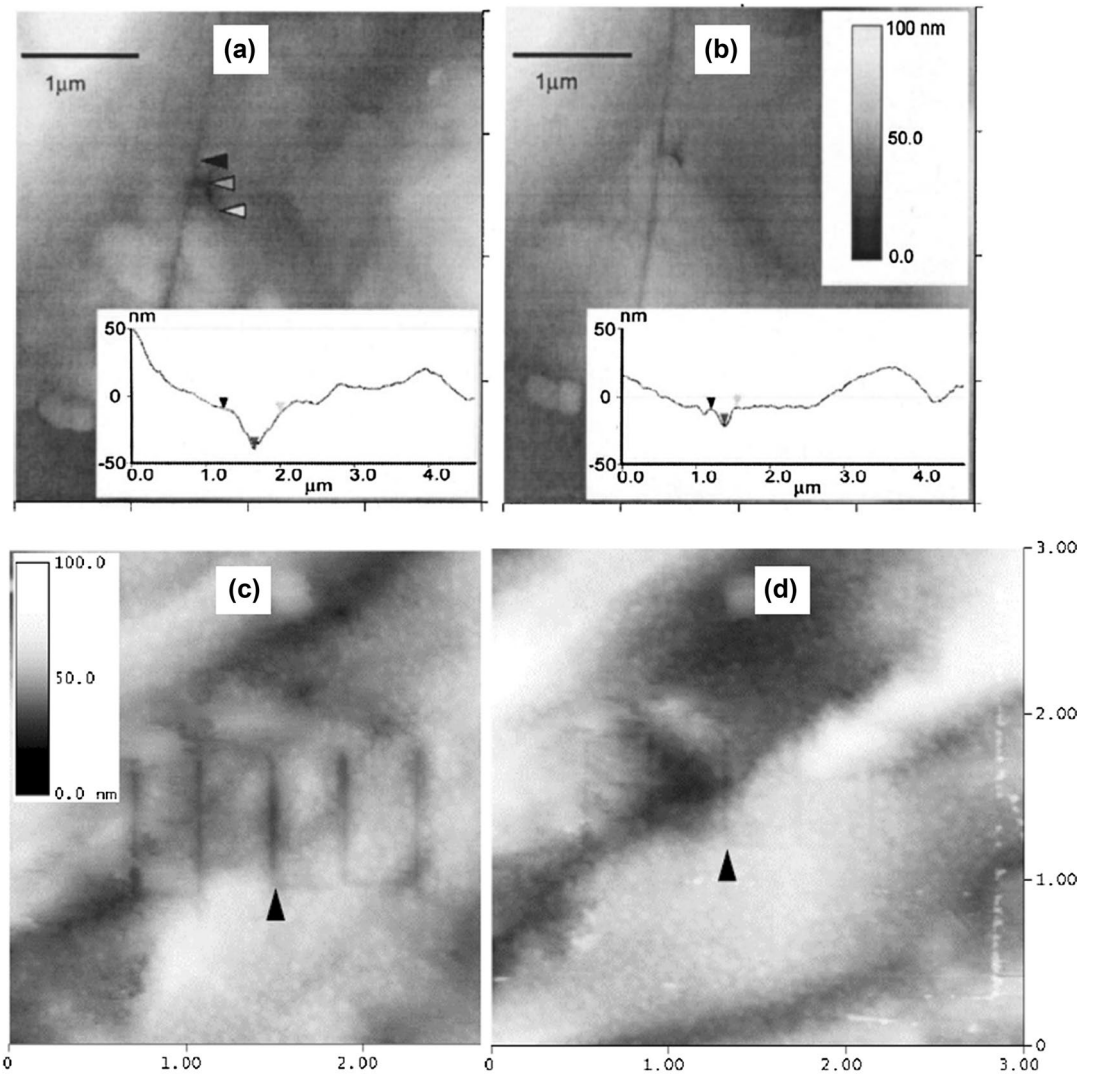J. Indian Inst. Sci.|VOL 102:1|211–235 January 2022|journal.iisc.ernet.in

Springer 🔷

Figure 10: AFM topographical maps of nanoindentation **a** before and **b** after heating a NiTi-based alloy specimen (reproduced with permission from[74]). AFM images of nano-scratch **c** before and **d** after heating[77].

into the NiTi specimen up to an indentation depth of 170 μm. Next, the whole fixture was kept in an oven for 2 min to reach a temperature of 423 ± 10 K. Further, it was quenched in ice water for 2 min to complete the training cycle. The 3D indent profile during heating and cooling were observed using optical surface profilometer and shown in Fig. 11a. The cross-sectional profiles of the heated and cooled indent impressions are shown in Fig. 11b. It is noticeable from the figure that heating to a temperature of ~400 K results to austenite phase, thereby leading to a significant depth recovery. Similar observations were also made by Fei et al. upon indentation and planarization of NiTi alloys[27]. They reported that martensitic NiTi alloys exhibited TW-SME when representative strain, i.e., ratio of the indent impression radius to the indenter radius (*a/r*) exceeded 0.25. The spherical indent impression appears to be shallow when the NiTi alloy is heated. On the other hand, the impression deepens upon cooling. Along with these studies, various literatures are available on characterizing SME in NiTi alloys and are in good agreement with these observations and theory[80,81].

3.2.2 Characterization of PE Behavior Using NI

For developing a deeper understanding about the small-scale deformation characteristics of NiTi alloys, Gall et al. employed instrumented microindentation on precipitated alloy system[82]. They

224

⌐ Springer

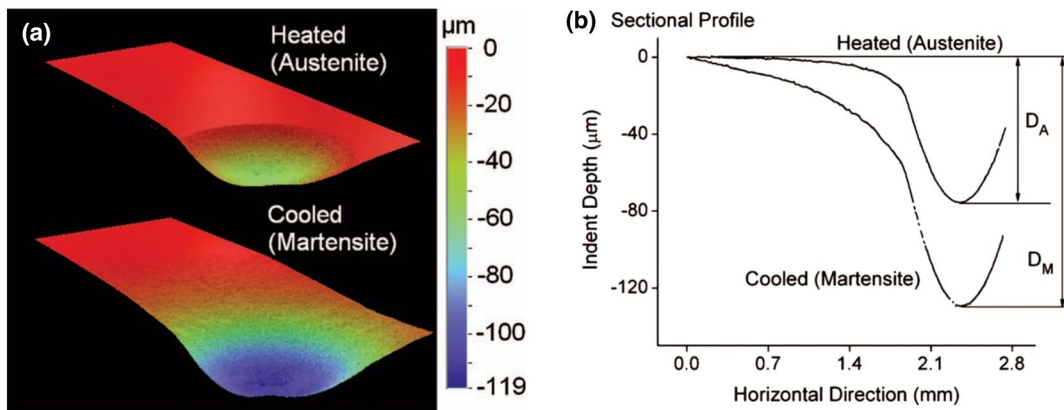J. Indian Inst. Sci.|VOL 102:1|211–235 January 2022|journal.iisc.ernet.in

Figure 11: a 3D profile of heated and cooled indent and **b** cross-sectional profile of heated and cooled indent (reproduced with permission from[79]).

have also complemented the investigation with thorough microstructural observations through TEM. The influence of different size scales (10–500 nm) of precipitates on the overall indentation response of the pseudoelastic NiTi system were systematically studied by them. The properties estimated using the $P–h$ curve, such as Vickers hardness (H_V) and recoverable energy (E_r), were used as the prime parameters to assess the degree of structural and functional behavior in the NiTi system. In fact, these properties indicate about the role played by dislocation-mediated plasticity and reversible stress-induced martensitic transformation in the deformation characteristics of NiTi system. Overall, higher values of H_V and E_r account for the superior structural and functional properties, respectively. Among the various precipitated NiTi system investigated in this study, a combination of highest H_V and E_r values were noted for NiTi alloy having smaller precipitates of size ~ 10 nm. The superior structural property for the alloy was attributed to the resistance exerted by the precipitate phases against the dislocation movement. On the other hand, the stress field around the precipitates reduced the critical applied stress required for SIMT. Presence of optimum sized precipitates thereby led to improved pseudoelasticity.

Nevertheless, a reduction in E_r was noted for the same NiTi alloy with intermediate precipitate sizes varying over 50–300 nm. It was noted that the presence of precipitates influenced the thermal characteristics of the alloy system, as well[82]. This in turn is related to the reduction in functional mechanism in the NiTi system with an increase in the precipitate size. In fact, the thermal characteristics revealed a higher transformation temperature for the NiTi alloy with

intermediate-sized precipitates in comparison to that for the small-sized one. Hence, the degree of reversible austenite to martensite transformation diminished and reduced the functional activities in the NiTi system, in case of the former.

Furthermore, Gall et al. analyzed the indentation response of the NiTi system consisting of significantly coarser precipitates of size ~ 500 nm as well[82]. Interestingly, such large-sized precipitates were noted to improve the structural and functional properties in the NiTi system. In fact, NiTi alloy with coarse precipitates underwent phase transformation at a lower temperature than that for the alloy consisting of intermediate-sized precipitates. It was realized that the large precipitates actually restricted the dislocation motion considerably and favored reversible SIMT activity within the indentation volume leading to simultaneous improvement in structural and functional properties at the same time. This disparity in the overall mechanical response of aged NiTi alloy consisting of different precipitate sizes originated from the variation in the size and shape of the precipitate morphology. This influenced the associated stress fields in the matrix. Overall, such a systematic study revealed the complex relationship between the mechanical behavior, microstructural features, and thermal characteristics of the NiTi system at the small scale. Certainly, such precise assessment benefitted in developing the thorough insight about the deformation micromechanism for NiTi alloy.

In another approach, Pfetzing et al. investigated the influence of crystallographic anisotropy on the indentation response of the NiTi system[83]. Accordingly, Berkovich indenter-based NI were performed on individual grains with respective
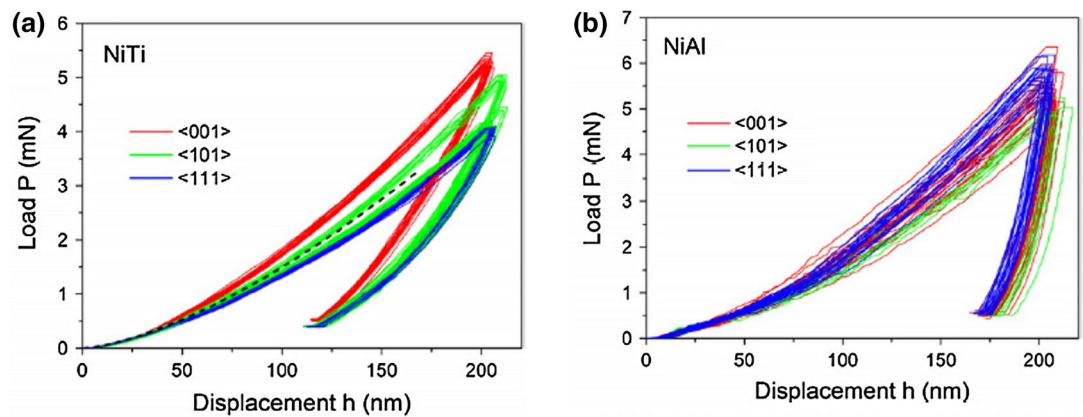
225

J. Indian Inst. Sci.|VOL 102:1|211–235 January 2022|journal.iisc.ernet.in   Springer

Figure 12: Load–displacement curves obtained upon nanoindenting grains oriented along three principal directions < 001 > , < 101 > and < 111 > for **a** austenitic NiTi (B2 crystal lattice) and **b** NiAl (B2 crystal lattice) alloys (reproduced with permission from[33]).

surface normal parallel to the principal orientations: < 111 > , < 110 > and < 100 >. Furthermore, they attempted to compare the unique pseudoelastic behavior of NiTi alloy with the typical elastic–plastic deformation trend for NiAl system. Figure 12 highlights the *P–h* responses for both the alloys. It is apparent from the Fig. 12a that the NiTi system depicted a strong orientation dependence in NI response. In fact, the applied load required to attain the desired indentation depth of 200 nm was noted to vary distinctly for the three different principal grain orientations. It is noteworthy that the < 100 > orientation required higher indentation load than that for < 110 > and < 111 > orientation. Significant depth recovery was also observed from the *P–h* curve of the NiTi system in comparison to that for the NiAl system. In fact, strong dependence of SIMT activity on the anisotropy of crystallographic orientation was evident from this investigation. Furthermore, the role played by stress triaxiality associated with NI was also highlighted by them in comparison to that for uniaxial micro-pillar compression[33]. In contrary, no prominent influence of crystallographic orientation on the indentation response was evident for the NiAl system. The alloy also showed significantly low depth recovery, as a characteristic for conventional elastic–plastic system (Fig. 12b). All these experimental observations and the predicted micro-mechanisms were validated by molecular dynamic simulations and *TEM*-based post-indentation analysis as well.

Furthermore, Laplanche et al. investigated the orientation dependency of SIMT in NiTi alloy using nanoindenter with axisymmetric spherical indenter $(R = 5 \ \mu m)$[84]. Similar to the previous study, principal orientations were considered for this investigation as well. In addition, a post-indentation analysis was performed by implementing AFM on the residual impression. This revealed the microstructural changes owing to indentation. Interestingly, it was noted that the residual imprints obtained upon indenting along the orientations [001], [101], and [111] showed variation in the symmetries. Figure 13 highlights different residual imprints captured from the principal orientation. These microstructural features, however, diminished upon heating the indented specimens above A_f. It was also observed that *SIMT* formation played an important role in sink-in formation in the NiTi system upon indentation, rather than inducing dislocation activities. The role of crystal orientation and SIMT in controlling the deformation mechanism and functional characteristics for the NiTi alloy are thereby further confirmed by these systematic investigations.

Apart from these highlighted studies, numerous research groups have explored the mechanical and functional behavior of NiTi-based SMAs at micron scale by implementing NI. These studies attempted to develop fundamental understanding about the micro-mechanisms associated with the deformation characteristics in the NiTi system by interpreting the *P–h* response with associated microstructural changes. However, quantitative assessment along with direct and prominent evidence of the SIMT characteristics from the *P–h* curves seemed challenging from these studies. This is primarily because deformation behavior of any material is conventionally assessed from the corresponding stress–strain behavior. In this regard, the recent efforts by Sujith et al.
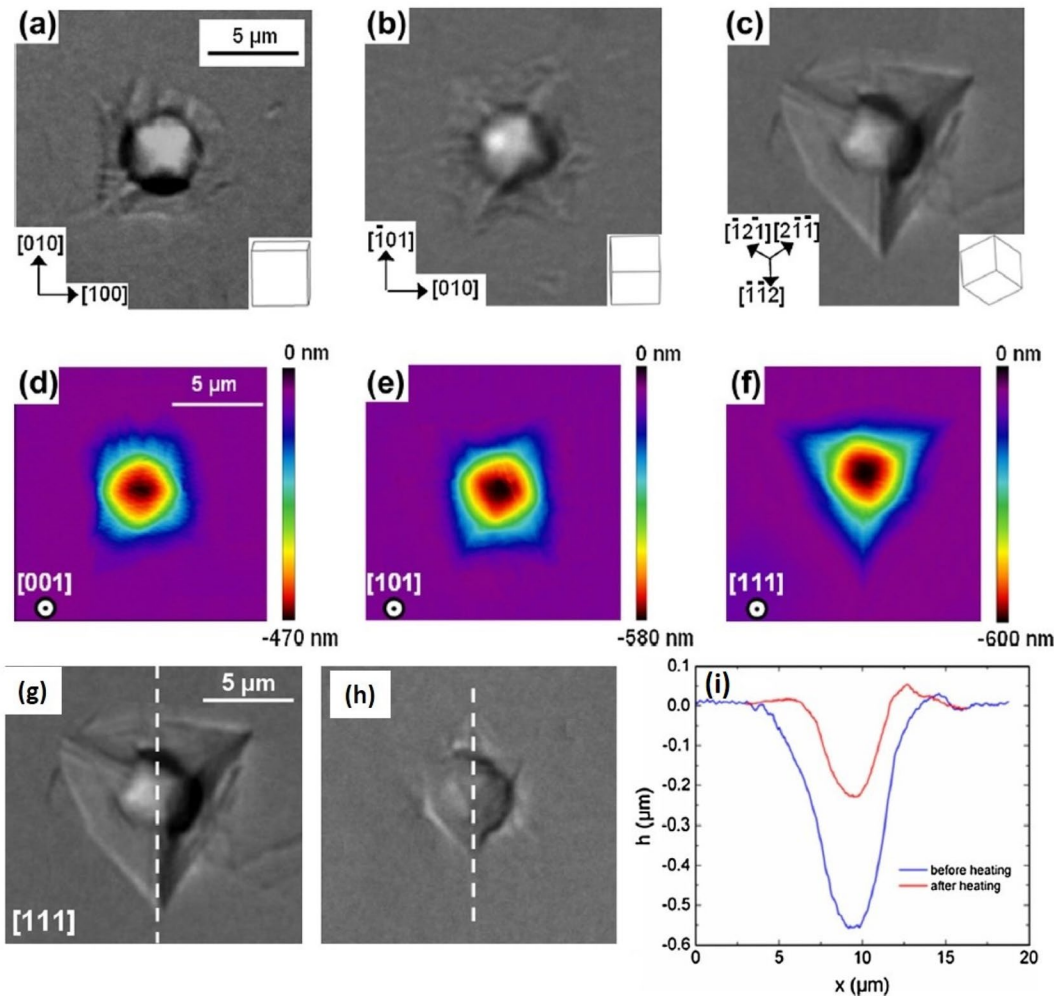
Figure 13: Optical micrographs of remnant indents from **a** [001], **b** [101] and **c** [111] oriented grains. Corresponding AFM images are shown in **d**, **e** and **f,** respectively. Optical micrograph showing **g** sink-in after nanoindentation tests and **h** disappearance of sink-in after heating above A_f. **i** Corresponding AFM depth profiles are also shown (reproduced with permission from[84]).

is mention worthy to bridge the gap and generate the stress–strain curves from NI of NiTi alloy system[16].

3.2.3 Evidence for SIMT from Nanoindentation P–h Curve

In the first attempt, the NI-based deformation response of not only NiTi system but also traditional and widely used ferrous and non-ferrous metallic systems such as ferritic stainless steel and aluminum were thoroughly explored and compared[63]. Interestingly, unique *P–h* characteristics with distinctly different slope, particularly during unloading was noted specifically for the NiTi system. Variation in the normalized indentation load vs. depth of penetration for all the studied alloys, nanoindented up to the same load level, using spherical tips are presented in Fig. 14a. Such normalization of unloading indentation load and indentation depth with corresponding maximum limit is widely employed to understand the role of different deformation mode on the indentation response of different materials[69]. The anomalous trend observed in case of NiTi alloy was attributed to the indentation-induced reversible austenite to martensitic phase transformation. A distinct evidence for the functional activity in the NiTi system in comparison to that for other ferrous and non-ferrous metallic systems was apparent from this investigation.

Furthermore, the research group intended to develop a *NI*-based protocol suitable for thoroughly characterizing the pseudoelasticity in NiTi system at small scale. This systematic study
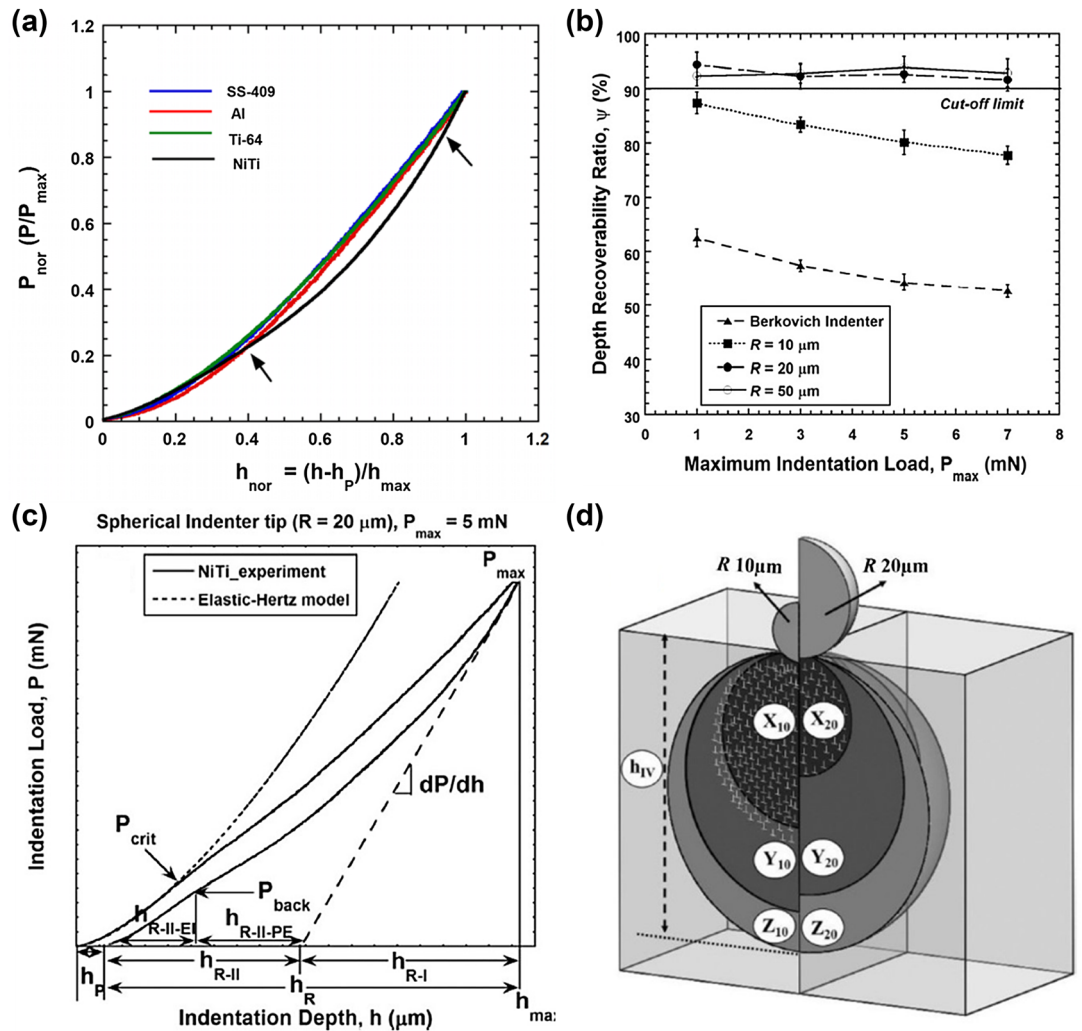
Springer

Figure 14: **a** Normalized instantaneous indentation load vs. normalized instantaneous remnant depth of indentation for NiTi alloy while nanoindented using spherical indenter (reproduced with permission from[85]). **b** Variation in depth recoverability ratio with P_{max} using Berkovich and spherical indenter tips. **c** Schematic representation of $P–h$ curve showing primary and secondary recoverable depths and **d** schematic representation of indentation volume generated using spherical indenter (reproduced with permission from[16]).

involved different geometry and sizes of indenter tip for nanoindenting NiTi alloy using varying load levels. Geometrically self-similar sharp Berkovich indenter as well as blunt spherical indenter with three different tip radii were used. To comprehend the overall indentation response of NiTi alloy with different indenter configurations, depth recoverability was measured from the $P–h$ curve. Estimation of this parameter accounted for a quantitative assessment for the degree of reversible mechanism. In case, the NiTi specimen was indented using a Berkovich tip, significantly lower depth recoverability (~45%) was noted. In fact, usage of sharp indenter led to dominant

dislocation activity. Consequently, the reversible phase transformation based recoverable mechanism subsided. On the contrary, depth recoverability as high as ~94% was achieved upon indenting the same alloy up to the same P_{max} but with a blunt spherical indenter having tip radius almost three orders of magnitude higher (see Fig. 14b). This observation indicated that conventionally used Berkovich indenter was not suitable for analyzing the deformation, particularly shape memory characteristics of the NiTi system. On the other hand, spherical indenter was apt to minimize the role of dislocation in the indentation volume and thereby to effectively assess the

228

🍃 Springer

J. Indian Inst. Sci.|VOL 102:1|211–235 January 2022|journal.iisc.ernet.in

recoverable pseudoelastic mechanism for NiTi alloy. In other words, the study rightly highlighted that the dominance of the SIMT-induced pseudoelasticity or the dislocation-mediated plasticity within the deformation volume was primarily controlled by the indentation parameters.

Based on this understanding, the authors focused to identify the optimum indentation parameters for assessing pseudoelasticity in NiTi-based SMA. NI was performed on the homogenized alloy using spherical indenter tip of radius, $R \sim 10$, 20, and 50 µm as well as varying maximum indentation load, P_{max} of 1–7 mN. Critical analysis of the P–h response for the alloy indicated that the dominant deformation mechanism can be differentiated into three categories: (i) elastic, (ii) pseudoelastic and (iii) plastic. In fact, the theoretical prediction of the P–h response based on the Hertzian relation was used to quantify the transition between the elastic to the pseudoelastic mechanism in the alloy, as illustrated through Fig. 14c. In the Figure, P_{crit} indicates the onset of SIMT in the indentation volume, and $h_{R-II-PE}$ signifies the depth of indentation purely influenced by SIMT. The authors performed a similar analysis on the P–h curve generated from varying indenter parameters and quantified the extent of different deformation modes present in the vicinity of the indenter. The deformation zones within the indentation volume are schematically shown in Fig. 14d. Also, strain-induced into the material in each case was estimated. Based on this quantitative analysis, the optimized indentation parameters, suitable for inducing prominent *SIMT* mechanism, resulting to significant depth recovery (>90%) were identified. Indentation using spherical indenter tip of $R = 20$ µm and P_{max} of 5 mN was confirmed as the best combination of parameters to assess the pseudoelasticity in the NiTi system. The study was first of a kind to report that pseudoelastic characteristics of NiTi-based system can be best appreciated only upon utilizing the optimized indentation conditions.

3.2.4 Converting P–h Curve to Indentation Stress–Indentation Strain Response

Subsequently, utilizing the optimized indentation parameters, a tailored protocol was formulated to convert the recorded P–h data into an indentation stress–strain (σ_{ind}–ε_{ind}) curve, particularly suitable for pseudoelastic NiTi system[16,86]. This novel protocol has been developed based on the pioneer study by Pathak et al. on generating the σ_{ind}–ε_{ind} curve of traditional elastic–plastic system[87–89]. In the analytical part, prior to conversion of P–h

curve into σ_{ind}–ε_{ind} curves, any effect of experimental artifact on the nanoindentation response was eliminated by pursuing 'zero-point correction'. Subsequently, P–h data were converted into indentation stress (σ_{ind})–indentation strain (ε_{ind}) using the following relation,

$$\sigma_{ind} = \frac{P}{\pi a^2}, \ \varepsilon_{ind} = \frac{h_r}{2.4a}, \tag{1}$$

$$a = \sqrt{Rh}. \tag{2}$$

This relationship was originated from the classical Hertzian elastic contact mechanics theory[16]. It is noteworthy that in traditional metallic system, the Hertzian relationship is valid up to the elastic limit, which can be judiciously used to predict the offset for the onset of SIMT in case of NiTi-based SMAs. This insight was utilized to generate indentation stress–strain curve for the alloy revealing all unique deformation features of pseudoelastic NiTi system including transformation strength, $\Delta\varepsilon_{pl}$, strain recovery, etc. as shown in Fig. 15a.

Further, this novel protocol was successfully utilized to trace the pseudoelastic characteristics of Laser Engineered Net Shaping-based additively manufactured (AM) NiTi system[90]. In this particular study, three different NiTi coupons produced using varying combination of processing parameters were investigated. Accordingly, along with the assessment of conventional mechanical properties such as H and E, using traditional micro- and nanoindentation with sharp indenter, indentation stress–strain curves were also generated from the spherical nanoindentation. Interestingly, it is observed that the measured H using sharp indenter did not show any noticeable variation with different processing condition for NiTi alloy. This is particularly noted upon employing indentation loads in macro-level. However, distinctly different trend was noted upon employing spherical nanoindentation-based investigation. This becomes particularly evident from the σ_{ind}–ε_{ind} curves. Schematic representation of σ_{ind}–ε_{ind} curve illustrating the critical forward (σ_{crit}) and backward transformation (σ_{back}) stresses as well as the range of maximum (ε_{max}), permanent (ε_P) and recoverable (ε_R) strains are shown in Fig. 15a. Variation in the σ_{ind}–ε_{ind} curves for the three different NiTi coupons produced with increasing laser energy densities are presented in Fig. 15b–d, respectively. Interestingly, evidence of pseudoelastic properties were noted only for the NiTi coupon manufactured with a specific combination of AM parameters. The study further validates the importance and applicability of characterizing
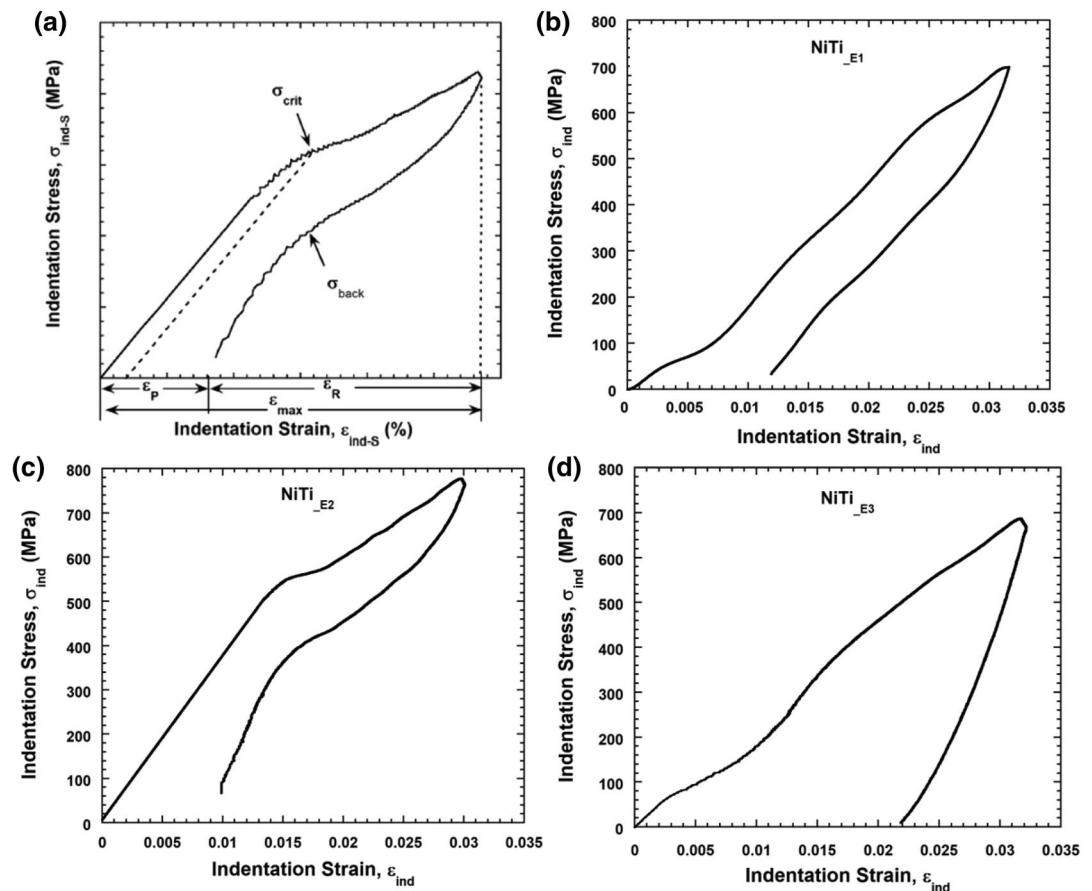
229

J. Indian Inst. Sci.|VOL 102:1|211–235 January 2022|journal.iisc.ernet.in

Figure 15: a Schematic representation of indentation stress–strain curve revealing critical transformation strength, σ_{crit} estimated as per 0.2% offset strain along with categorization of maximum strain, ε_{max} to plastic strain, ε_P and recoverable strain, ε_R. **b** Indentation stress–strain curve for NiTi$_{E1}$ **c** for NiTi$_{E2}$ and **d** for NiTi$_{E3}$ alloys (reproduced with permission from[76]).

stress–strain behavior of NiTi alloy at small scale, through *NI* for assessing the deformation micro-mechanisms.

All these studies have essentially paved the way to characterize the NiTi system at sub-micron scale. Particularly, the latest development of NI using spherical indenter and its post-indentation analysis specifically for the PE-NiTi system is considered as a breakthrough for broader investigations at such a small scale.

3.3 Challenges in Micro-mechanical Testing of NiTi-Based SMA

The previous sections have highlighted the remarkable studies in the field of small-scale testing on NiTi-based shape memory alloys. These research attempts have certainly provided a scientific basis to comprehend the micro-mechanism behind the shape memory properties of NiTi-based system. However, it is important to understand that implementing a characterizing tool

like micro-pillar compression and nanoindentation is associated with a number of challenges. As elaborated earlier, fabricating and deforming the micro-pillar requires sophisticated equipment and utmost care. This practical difficulty has restricted the handy usage of micro-pillar tests in most of the research studies in the field of shape memory alloys as well as on the other alloy systems. On the other hand, recent development in nanoindentation with a tailored protocol for generating the σ_{ind}–ε_{ind} curves is observed to be a substitute to micro-pillar compression test. In this nanoindentation-based approach, all major signature characteristics of pseudoelasticity, as evident from the conventional uniaxial test are replicated in the σ_{ind}–ε_{ind} curve. Even though, the existence of the multi-axial state of stress along with constraint nature of the nanoindentation leads to overestimation of transformation properties in comparison to conventional uniaxial test. Such anomaly and restrictions in the assessment

230

Springer

J. Indian Inst. Sci.|VOL 102:1|211–235 January 2022|journal.iisc.ernet.in

techniques lead to uncertainty in the evaluation process at small scale. Future studies should be directed to address these disparities for the complex system of NiTi. The variation between the properties, assessed upon applying uniaxial stress through conventional tensile/compression tests and multi-axial state of stress, generated by nanoindentation will be informative from a scientific point of view.

Requirement of optimized indenter tip is considered as the practical limitation in implementing a novel nanoindentation-based protocol for future studies on pseudoelastic NiTi systems. Furthermore, it is crucial to understand that micro-pillar compression and nanoindentation are compressive in nature. Therefore, a characterization tool that can provide the tensile characteristics on a small scale has the potential to provide a more scientific basis to this shape memory system. It is imperative because asymmetry in tension–compression behavior is reported in a number of studies on NiTi system[91]. Nevertheless, the development of an experimental method with the capability to assess fatigue behavior has huge importance for the wider deployment of alloy in miniaturized applications.

4 Summary

The article presents an extensive review for the deformation behavior of NiTi-based shape memory alloys, assessed through micro-mechanical testing. Elementary mechanisms behind the shape memory properties of the NiTi system are elaborated in detail to develop an insight about this unique material system. Evaluation of the structural and functional characteristics of NiTi alloy at the sub-micron scale, pursued through micro-pillar compression and nanoindentation-based investigations and the associated micro-mechanism of deformation are reported in this article. It is noted that the stress–strain curves, obtained from micro-pillar compression reveal significant strain recovery for NiTi alloys, thereby confirming the pseudoelastic characteristics even at micron- and sub-micron scale. The state-of-the-art research investigating the influence of crystallographic orientation, presence of precipitate phases and even specimen size on this pseudoelastic behavior at the micro/nano-scale are highlighted. Nevertheless, micro-pillar compression test is associated with challenging specimen preparation technique that affects the characterized properties as well. On the other hand, user-friendly nanoindentation technique has gained a wide applicability to assess the mechanical

behavior of NiTi-based shape memory alloys at the micro- or even sub-micro-scale. Several groups have attempted to explore the different properties of the NiTi system by varying the experimental parameters including indenter tip configurations as well as indentation load, depth of penetration etc. Interestingly, such flexibility in nanoindentation technique has been evolved to a stage to generate stress–strain characteristics for the NiTi system along with conventional hardness and elastic moduli measurement. This development in the nanoindentation technique is a breakthrough for the characterization of the pseudoelastic NiTi system at a small scale. A detailed overview about the micro-mechanisms of the deformation behavior of NiTi-based shape memory alloys can be obtained from this review.

Declarations

Conflict of interest

On behalf of all authors, the corresponding author states that there is no conflict of interest.

References

1. Senthilnathan K (2010) Pseudoelastic shape memory alloy model with stent deployment simulation. ProQuest Dissertations Publishing, State University of New York at Buffalo, USA
2. Otsuka K, Ren X (2005) Physical metallurgy of Ti–Ni-based shape memory alloys. Prog Mater Sci 50:511–678. https://doi.org/10.1016/j.pmatsci.2004.10.001
3. Stoeckel D, Melzer A (1995) The use of niti alloys for surgical instruments. In: Materials in clinical applications, pp 791–798. www.nitinol.com

231

J. Indian Inst. Sci.|VOL 102:1|211–235 January 2022|journal.iisc.ernet.in   ⌂ Springer

4. Mehrpouya M, Bidsorkhi HC (2017) MEMS applications of NiTi based shape memory alloys: a review. Micro Nanosyst 8:79–91. https://doi.org/10.2174/1876402908666161102151453

5. Ozbulut OE, Daghash S, Sherif MM (2016) Shape memory alloy cables for structural applications. J Mater Civ Eng 28:04015176. https://doi.org/10.1061/(asce)mt.1943-5533.0001457

6. Quan D, Hai X (2015) Shape memory alloy in various aviation field. Proc Eng 99:1241–1246. https://doi.org/10.1016/j.proeng.2014.12.654

7. Csanádi T, Naughton-Duszová A, Dusza J (2018) Anisotropic slip activation via homogeneous dislocation nucleation in ZrB2 ceramic grains during nanoindentation. Scr Mater 152:89–93. https://doi.org/10.1016/j.scriptamat.2018.04.025

8. Jacob K, Yadav D, Dixit S, Hohenwarter A, Jaya BN (2021) High pressure torsion processing of maraging steel 250: microstructure and mechanical behaviour evolution. Mater Sci Eng A 802:140665. https://doi.org/10.1016/j.msea.2020.140665

9. Ozdemir N, Karaman I, Mara NA, Chumlyakov YI, Karaca HE (2012) Size effects in the superelastic response of Ni 54Fe 19Ga 27 shape memory alloy pillars with a two stage martensitic transformation. Acta Mater 60:5670–5685. https://doi.org/10.1016/j.actamat.2012.06.035

10. Bhargava AK, Sharma CP (2011) Mechanical behaviour and testing of materials. Prentice Hall India Learning Private Limited, India

11. François D, Pineau A, Zaoui A (1998) Mechanical behaviour of materials. Springer, Netherlands

12. Shetty MN (2013) Dislocations and mechanical behaviour of materials. Prentice Hall India Learning Private Limited, India

13. Hopulele I, Istrate S, Stanciu S, Calugaru G (2004) Comparative study of certain Cu-Zn-Al-type alloys concerning their superelastic behavior and shape memory. J Optoelectron Adv Mater 6:277–282

14. Gall K, Sehitoglu H, Chumlyakov YI, Kireeva IV (1999) Tension-compression asymmetry of the stress-strain response in aged single crystal and polycrystalline NiTi. Acta Mater 47:1203–1217. https://doi.org/10.1016/S1359-6454(98)00432-7

15. Patoor E, Lagoudas DC, Entchev PB, Brinson LC, Gao X (2006) Shape memory alloys, part I: general properties and modeling of single crystals. Mech Mater 38:391–429. https://doi.org/10.1016/j.mechmat.2005.05.027

16. Kumar S, Kumar IA, Marandi L, Sen I (2020) Assessment of small-scale deformation characteristics and stress-strain behavior of NiTi based shape memory alloy using nanoindentation. Acta Mater 201:16375. https://doi.org/10.1016/j.actamat.2020.09.080

17. Young ML, Wagner MFX, Frenzel J, Schmahl WW, Eggeler G (2010) Phase volume fractions and strain measurements in an ultrafine-grained NiTi shape-memory alloy during tensile loading. Acta Mater 58:2344–2354. https://doi.org/10.1016/j.actamat.2009.12.021

18. Ahadi A, Sun Q (2013) Stress hysteresis and temperature dependence of phase transition stress in nanostructured NiTi—effects of grain size. Appl Phys Lett. https://doi.org/10.1063/1.4812643

19. Elibol C, Wagner MFX (2015) Investigation of the stress-induced martensitic transformation in pseudoelastic NiTi under uniaxial tension, compression and compression-shear. Mater Sci Eng A 621:76–81. https://doi.org/10.1016/j.msea.2014.10.054

20. Saburi T, Yoshida M, Nenno S (1984) Deformation behavior of shape memory Ti-Ni alloy crystal. Scr Metall 18:363–366

21. Basu R, Jain L, Maji BC, Krishnan M, Mani Krishna KV, Samajdar I, Pant P (2012) Origin of microstructural irreversibility in Ni-Ti based shape memory alloys during thermal cycling. Metall Mater Trans A Phys Metall Mater Sci 43:1277–1287. https://doi.org/10.1007/s11661-011-0970-y

22. Kumar PK, Lagoudas DC (2010) Shape memory alloys. Shape Mem Alloy. https://doi.org/10.1007/978-0-387-47685-8-1

23. Superelastic tire (n.d.). https://technology.nasa.gov/patent/LEW-TOPS-99

24. Van Humbeeck J (1999) Non-medical applications of shape memory alloys. Mater Sci Eng A 273:134–148. https://doi.org/10.1016/S0921-5093(99)00293-2

25. Garay JE, Anselmi-Tamburini U, Munir ZA (2003) Enhanced growth of intermetallic phases in the Ni-Ti system by current effects. Acta Mater 51:4487–4495. https://doi.org/10.1016/S1359-6454(03)00284-2

26. Thompson SA (2000) An overview of nickel-titanium alloys used in dentistry. Int Endod J 33:297–310. https://doi.org/10.1046/j.1365-2591.2000.00339.x

27. Fei X, Connell CJO, Grummon DS, Cheng YT (2011) Surface form memory by indentation and planarization of NiTi: displacements and mechanical energy density during constrained recovery. J Mater Sci 46:7401–7409. https://doi.org/10.1007/s10853-011-5702-6

28. Zhou Y, Zhang J, Fan G, Ding X, Sun J, Ren X, Otsuka K (2005) Origin of 2-stage R-phase transformation in low-temperature aged Ni-rich Ti-Ni alloys. Acta Mater 53:5365–5377. https://doi.org/10.1016/j.actamat.2005.08.013

29. Khalil-Allafi J, Dlouhy A, Eggeler G (2002) Ni4Ti3-precipitation during aging of NiTi shape memory alloys and its influence on martensitic phase transformations. Acta Mater 50:4255–4274. https://doi.org/10.1016/S1359-6454(02)00257-4

30. Dey SK, Sen I, Samanta S (2021) Mechanical characterisation of PEEK-HA composite as an orthopaedic implant. Adv Mater Process Technol. https://doi.org/10.1080/2374068X.2021.1970990

31. Kousbroek R (1990) Shape memory alloys. In: ASM Handbook, Prop. Sel. Nonferrous Alloy. Spec. Mater., vol 2, pp 897–902. https://doi.org/10.1201/9781351074438

32. Mentz J, Frenzel J, Wagner MFX, Neuking K, Eggeler G, Buchkremer HP, Stöver D (2008) Powder metallurgical processing of NiTi shape memory alloys with elevated transformation temperatures. Mater Sci Eng A 491:270–278. https://doi.org/10.1016/j.msea.2008.01.084

33. Hodgson DE, Biermann RJ (1990) Shape memory alloys. In: ASM Handbook, Prop. Sel. Nonferrous Alloy. Spec. Mater., vol 2, pp 897–901. https://doi.org/10.1201/97813 51074438

34. Jiang SY, Zhao YN, Zhang YQ, Hu L, Liang YL (2013) Effect of solution treatment and aging on microstructural evolution and mechanical behavior of NiTi shape memory alloy. Trans Nonferrous Met Soc China (English Ed) 23:3658–3667. https://doi.org/10.1016/S1003-6326(13) 62914-3

35. Wadood A (2016) Brief overview on nitinol as biomaterial. Adv Mater Sci Eng. https://doi.org/10.1155/2016/ 4173138

36. Duerig TW, Bhattacharya K (2015) The Influence of the R-phase on the superelastic behavior of NiTi. Shape Mem Superelast 1:153–161. https://doi.org/10.1007/ s40830-015-0013-4

37. Huang X, Ackland GJ, Rabe KM (2003) Crystal structures and shape-memory behaviour of NiTi. Nat Mater 2:307–311. https://doi.org/10.1038/nmat884

38. Khalil-Allafi J, Schmahl WW, Toebbens DM (2006) Space group and crystal structure of the R-phase in binary NiTi shape memory alloys. Acta Mater 54:3171–3175. https:// doi.org/10.1016/j.actamat.2006.02.040

39. Bataillard L, Bidaux J, Gotthardt R (2009) Interaction between microstructure and multiple- step transformation in binary NiTi alloys using in-situ transmission electron microscopy observations. Philos Mag A. https://doi. org/10.1080/01418619808241907

40. Gall K, Sehitoglu H (2012) The role of texture in tension±compression asymmetry in polycrystalline NiTi. Int J Plast 15:1–24

41. Arciniegas M, Casals J, Manero JM, Peña J, Gil FJ (2008) Study of hardness and wear behaviour of NiTi shape memory alloys. J Alloys Compd 460:213–219. https://doi. org/10.1016/j.jallcom.2007.05.069

42. Bhagyaraj J, Ramaiah KV, Saikrishna CN, Bhaumik SK (2013) Gouthama, behavior and effect of Ti2Ni phase during processing of NiTi shape memory alloy wire from cast ingot. J Alloys Compd 581:344–351. https://doi.org/ 10.1016/j.jallcom.2013.07.046

43. Buehler WJ, Gilfrich JV, Wiley RC (1963) Effect of low-temperature phase changes on the mechanical properties of alloys near composition TiNi. J Appl Phys 34:1475–1477. https://doi.org/10.1063/1.1729603

44. Zou WH, Han XD, Wang R, Zhang Z, Zhang WZ, Lai JKL (1996) TEM and HREM study of the interphase interface structure of Ti3Ni4 precipitates and parent phase in an aged TiNi shape memory alloy. Mater Sci Eng A 219:142–147. https://doi.org/10.1016/S0921-5093(96)10418-4

45. Carroll MC, Somsen C, Eggeler G (2004) Multiple-step martensitic transformations in Ni-rich NiTi shape memory alloys. Scr Mater 50:187–192. https://doi.org/10. 1016/j.scriptamat.2003.09.020

46. Fei H, Abraham A, Chawla N, Jiang H (2012) Evaluation of micro-pillar compression tests for accurate determination of elastic-plastic constitutive relations. J Appl Mech 79:061011. https://doi.org/10.1115/1.4006767

47. Greer JR, De Hosson JTM (2011) Plasticity in small-sized metallic systems: intrinsic versus extrinsic size effect. Prog Mater Sci 56:654–724. https://doi.org/10.1016/j.pmatsci. 2011.01.005

48. Dehm G, Jaya BN, Raghavan R, Kirchlechner C (2018) Overview on micro- and nanomechanical testing: new insights in interface plasticity and fracture at small length scales. Acta Mater 142:248–282. https://doi.org/10.1016/j. actamat.2017.06.019

49. Greer JR, Oliver WC, Nix WD (2005) Size dependence of mechanical properties of gold at the micron scale in the absence of strain gradients. Acta Mater 53:1821–1830. https://doi.org/10.1016/j.actamat.2004.12.031

50. Uchic MD, Dimiduk DM, Florando JN, Nix WD (2004) Sample dimensions influence strength and crystal plasticity. Science (80-) 305:986–989. https://doi.org/10.1126/ science.1098993

51. Greer JR, Weinberger CR, Cai W (2008) Comparing the strength of f.c.c. and b.c.c. sub-micrometer pillars: compression experiments and dislocation dynamics simulations. Mater Sci Eng A 493:21–25. https://doi.org/10. 1016/j.msea.2007.08.093

52. Hou XD, Bushby AJ, Jennett NM (2008) Study of the interaction between the indentation size effect and Hall-Petch effect with spherical indenters on annealed polycrystalline copper. J Phys D Appl Phys 41:74006

53. Leitner A, Maier-Kiener V, Kiener D (2017) Extraction of flow behavior and Hall-Petch parameters using a nanoindentation multiple sharp tip approach. Adv Eng Mater 19:1600669

54. Lehto P, Remes H, Saukkonen T, Hänninen H, Romanoff J (2014) Influence of grain size distribution on the Hall-Petch relationship of welded structural steel. Mater Sci Eng A 592:28–39

55. Frick CP, Orso S, Arzt E (2007) Loss of pseudoelasticity in nickel-titanium sub-micron compression pillars. Acta Mater 55:3845–3855. https://doi.org/10.1016/j.actamat. 2007.02.034

56. Manjeri RM, Qiu S, Mara N, Misra A, Vaidyanathan R (2010) Superelastic response of [111] and [101] oriented NiTi micropillars. J Appl Phys. https://doi.org/10.1063/1. 3445262

57. Juan JS, Nó ML, Schuh CA (2009) Nanoscale shape-memory alloys for ultrahigh mechanical damping. Nat

J. Indian Inst. Sci.|VOL 102:1|211–235 January 2022|journal.iisc.ernet.in

233

Nanotechnol 4:415–419. https://doi.org/10.1038/nnano.2009.142

58. Pfetzing-Micklich J, Ghisleni R, Simon T, Somsen C, Michler J, Eggeler G (2012) Orientation dependence of stress-induced phase transformation and dislocation plasticity in NiTi shape memory alloys on the micro scale. Mater Sci Eng A 538:265–271. https://doi.org/10.1016/j.msea.2012.01.042

59. Ye J, Mishra RK, Pelton AR, Minor AM (2010) Direct observation of the NiTi martensitic phase transformation in nanoscale volumes. Acta Mater 58:490–498. https://doi.org/10.1016/j.actamat.2009.09.027

60. Clarke AJ, Field RD, Dickerson PO, McCabe RJ, Swadener JG, Hackenberg RE, Thoma DJ (2009) A microcompression study of shape-memory deformation in U-13 at.% Nb. Scr Mater 60:890–892. https://doi.org/10.1016/j.scriptamat.2009.02.003

61. Norfleet DM, Sarosi PM, Manchiraju S, Wagner MFX, Uchic MD, Anderson PM, Mills MJ (2009) Transformation-induced plasticity during pseudoelastic deformation in Ni-Ti microcrystals. Acta Mater 57:3549–3561. https://doi.org/10.1016/j.actamat.2009.04.009

62. Frick CP, Clark BG, Schneider AS, Maaß R, Van Petegem S, Van Swygenhoven H (2010) On the plasticity of small-scale nickel-titanium shape memory alloys. Scr Mater 62:492–495. https://doi.org/10.1016/j.scriptamat.2009.12.023

63. Clark BG, Gianola DS, Kraft O, Frick CP (2010) Size independent shape memory behavior of nickel-titanium. Adv Eng Mater 12:808–815. https://doi.org/10.1002/adem.201000048

64. Paul PP, Kabirifar P, Sun Q, Brinson LC (2019) Structure-microstructure interactions in compression deformation of NiTi shape memory alloy micropillars. Mater Lett 257:126693. https://doi.org/10.1016/j.matlet.2019.126693

65. Gall K, Sehitoglu H, Anderson R, Karaman I, Chumlyakov YI, Kireeva IV (2001) On the mechanical behavior of single crystal NiTi shape memory alloys and related polycrystalline phenomenon. Mater Sci Eng A 317:85–92

66. Frick CP, Clark BG, Orso S, Sonnweber-Ribic P, Arzt E (2008) Orientation-independent pseudoelasticity in small-scale NiTi compression pillars. Scr Mater 59:7–10. https://doi.org/10.1016/j.scriptamat.2008.01.051

67. San Juan JM, Nó ML, Schuh CA (2008) Superelasticity and shape memory in micro- and nanometer-scale pillars. Adv Mater 20:272–278. https://doi.org/10.1002/adma.200701527

68. Pfetzing-Micklich J, Wagner MFX, Zarnetta R, Frenzel J, Eggeler G, Markaki AE, Wheeler J, Clyne TW (2010) Nanoindentation of a pseudoelastic NiTiFe shape memory alloy. Adv Eng Mater 12:13–19. https://doi.org/10.1002/adem.200900266

69. Oliver WC, Pharr GM (2004) Measurement of hardness and elastic modulus by instrumented indentation: Advances in understanding and refinements to

70. Murase K, Morrison KL, Tam PY, Stafford RL, Jurnak F, Weiss GA (2003) EF-Tu binding peptides identified, dissected, and affinity optimized by phage display GDP conformation of EF-Tu. Because EF-Tu is abundant in the cell, other functions have been suggested, particularly during periods of cellular stress when protein syn-g. Chem Biol 10:161–168

71. Il Jang J, Lance MJ, Wen S, Tsui TY, Pharr GM (2005) Indentation-induced phase transformations in silicon: influences of load, rate and indenter angle on the transformation behavior. Acta Mater 53:1759–1770. https://doi.org/10.1016/j.actamat.2004.12.025

72. Field JS, Swain MV (1993) A simple predictivity model for spherical indentation. J Mater Res 8:297–306. https://doi.org/10.1557/JMR.1993.0297

73. Muir Wood AJ, Sanjabi S (2008) Nanoindentation of binary and ternary Ni-Ti-based shape memory alloy thin films. Surf Coat Technol 202:3115–3120. https://doi.org/10.1016/j.surfcoat.2007.11.011

74. Shaw GA, Stone DS, Johnson AD, Ellis AB, Crone WC (2003) Shape memory effect in nanoindentation of nickel-titanium thin films. Appl Phys Lett 83:257–259. https://doi.org/10.1063/1.1591235

75. Yan W, Sun Q, Feng XQ, Qian L (2007) Analysis of spherical indentation of superelastic shape memory alloys. Int J Solids Struct 44:1–17. https://doi.org/10.1016/j.ijsolstr.2006.04.007

76. Amini A, He Y, Sun Q (2011) Loading rate dependency of maximum nanoindentation depth in nano-grained NiTi shape memory alloy. Mater Lett 65:464–466. https://doi.org/10.1016/j.matlet.2010.10.026

77. Crone WC, Shaw GA, Stone DS, Johnson AD, Ellis AB (2003) Shape recovery after nanoindentation of NiTi thin films. In: 2003 SEM Annu. Conf. Expo. Exp. Appl. Mech., pp 1–6

78. Li P, Karaca HE, Cheng YT (2017) Rapid characterization of local shape memory properties through indentation. Sci Rep 7:1–8. https://doi.org/10.1038/s41598-017-13434-9

79. Zhang Y, Cheng YT, Grummon DS (2006) Two-way indent depth recovery in a NiTi shape memory alloy. Appl Phys Lett 88:3–5. https://doi.org/10.1063/1.2189201

80. Laursen CM, Peter NJ, Gerstein G, Maier HJ, Dehm G, Frick CP (2020) Influence of Ti3Ni4 precipitates on the indentation-induced two-way shape-memory effect in Nickel-Titanium. Mater Sci Eng A 792:139373. https://doi.org/10.1016/j.msea.2020.139373

81. Su JF, Huang WM, Hong MH (2007) Indentation and two-way shape memory in a NiTi polycrystalline shape-memory alloy. Smart Mater Struct. https://doi.org/10.1088/0964-1726/16/1/S14

82. Gall K, Juntunen K, Maier HJ, Sehitoglu H, Chumlyakov YI (2001) Instrumented micro-indentation of NiTi

234

⌕ Springer

J. Indian Inst. Sci.|VOL 102:1|211–235 January 2022|journal.iisc.ernet.in

shape-memory alloys. Acta Mater 49:3205–3217. https://doi.org/10.1016/S1359-6454(01)00223-3

83. Pfetzing-Micklich J, Somsen C, Dlouhy A, Begau C, Hartmaier A, Wagner MFX, Eggeler G (2013) On the crystallographic anisotropy of nanoindentation in pseudoelastic NiTi. Acta Mater 61:602–616. https://doi.org/10.1016/j.actamat.2012.09.081

84. Laplanche G, Pfetzing-Micklich J, Eggeler G (2014) Orientation dependence of stress-induced martensite formation during nanoindentation in NiTi shape memory alloys. Acta Mater 68:19–31. https://doi.org/10.1016/j.actamat.2014.01.006

85. Sujith Kumar S, Sen I (2021) A comparative study on deformation behaviour of superelastic NiTi with traditional elastic-plastic alloys in sub-micron scale. Trans Indian Inst Met. https://doi.org/10.1007/s12666-021-02207-8

86. Sen I, Sujith Kumar S (2021) Characterizing stress-strain behavior of materials through nanoindentation. INTECH. https://doi.org/10.5772/intechopen.98495

87. Pathak S, Kalidindi SR (2015) Spherical nanoindentation stress-strain curves. Mater Sci Eng R Rep 91:1–36. https://doi.org/10.1016/j.mser.2015.02.001

88. Pathak S, Shaffer J, Kalidindi SR (2009) Determination of an effective zero-point and extraction of indentation stress-strain curves without the continuous stiffness measurement signal. Scr Mater 60:439–442. https://doi.org/10.1016/j.scriptamat.2008.11.028

89. Kalidindi SR, Pathak S (2008) Determination of the effective zero-point and the extraction of spherical nanoindentation stress-strain curves. Acta Mater 56:3523–3532. https://doi.org/10.1016/j.actamat.2008.03.036

90. Kumar S, Marandi L, Balla VK, Bysakh S, Piorunek D, Eggeler G, Das M, Sen I (2019) Microstructure—property correlations for additively manufactured NiTi based shape memory alloys. Materialia 8:100456. https://doi.org/10.1016/j.mtla.2019.100456

91. Šittner P, Heller L, Pilch J, Curfs C, Alonso T, Favier D (2014) Young's modulus of austenite and martensite phases in superelastic NiTi wires. J Mater Eng Perform. https://doi.org/10.1007/s11665-014-0976-x

S. Sujith Kumar is currently working as a post-doctoral researcher at the Metallurgical Engineering and Materials Science, Indian Institute of Technology- Bombay, India. IIT Bombay awarded him a prestigious Institute post-doctoral fellowship (IPDF) in 2020 for his post-doctoral position. He received his doctoral degree from the Department of Metallurgical and materials engineering, Indian Institute of Technology- Kharagpur, India, in 2020. His Ph.D. research was mainly focused on the 'Deformation behavior of NiTi based shape memory alloys at the sub-micron scale'. Prior to his Ph.D., he completed his Bachelor's degree in Mechanical Engineering from Kerala University in 2011. Subsequently, he pursued his Master's degree in Industrial Metallurgy from the National Institute of Technology, Tiruchirappalli, in 2014. Thereafter, he worked as an Assistant Professor in the Department of Mechanical Engineering, College of Engineering Kallooppara, Kerala, till Jan 2015. His research interest includes analysis of functional property variation in shape memory alloys, nanoindentation-based mechanical property analysis, microstructure property correlation of additive manufactured NiTi based alloys, and study on the mechanical property variation in Fe-based bulk metallic glasses.

Adya Charan Arohi is a Doctoral Research Scholar at the Department of Metallurgical and Materials Engineering, Indian Institute of Technology Kharagpur. Currently, he is involved in developing the "microstructure-property correlation of high strength metastable beta titanium alloy" since Jan 2018. Earlier, he received his Master in Technology (M.Tech) degree from the Department of Metallurgical and Materials Engineering, National Institute of Technology Warangal in June 2017. During his M.Tech, he has carried out his dissertation work on evaluating the "Multiaxial fatigue behaviour of near alpha titanium alloy for aeroengine applications" at Defence Metallurgical Research Laboratory, Hyderabad. Prior to his M.Tech, he has graduated from Gurukul Kangri Vishwavidayalaya, Haridwar with a bachelor degree (B.Tech) in the Department of Mechanical Engineering in June 2014. His scientific contributions include one research article, one conference paper and two conference presentations.

Indrani Sen is an Associate Professor at the Department of Metallurgical and Materials Engineering, IIT Kharagpur. She graduated (with a Doctoral degree) from the Department of Materials Engineering, Indian Institute of Science, Bangalore in 2010. Prior to that she completed M.Tech. from IIT Kharagpur (2005) and received Institute silver medal as the topper from the Materials Science Center. Following Ph.D., she pursued post-doctoral research at Chemnitz University of Technology, Germany and has bagged the prestigious Alexander von Humboldt (AvH) Fellowship. She also held visiting faculty and Av-Humboldt renewed research stay positions at University of Tennessee, USA (2016) and Ruhr University, Bochum, Germany (2018). Dr. Sen has made some notable contribution in the field of fracture, fatigue and failure of different category of conventionally produced, thermomechanical processed as well as state of the art additively manufactured materials which are promising candidates for aerospace, marine and biomedical applications. So far, she has managed to showcase her research globally through various National and International conferences, Workshops and Faculty Development Programs (around 30) as well as made around 30 International Peer Reviewed Journal publications including Acta Materialia, Scripta Materialia, Materialia etc. and book chapter.

J. Indian Inst. Sci.|VOL 102:1|211–235 January 2022|journal.iisc.ernet.in

Springer

235